

# 國立交通大學

電信工程學系碩士班

碩士論文

對稱式光柵耦合器之寬頻研究

**Clarification of Wideband Grating Couplers  
with Symmetrical Profiles**

研究生：曾凱悌

指導教授：彭松村 博士

黃瑞彬 博士

中華民國九十三年七月

對稱式光柵耦合器之寬頻研究

Clarification of Wideband Grating Couplers with Symmetrical Profiles

研究生：曾凱悌

Student: Kai-Ti Tseng

指導教授：彭松村 博士

Advisor: Dr. Song-Tsuen Peng

黃瑞彬 博士

Dr. Ruey-Bing Hwang

國立交通大學

電信工程學系碩士班

碩士論文



Submitted to Department of Communication Engineering

College of Electrical Engineering and Computer Science

National Chiao Tung University

In Partial Fulfillment of the Requirements

for the Degree of

Master of Science

in

Electrical Engineering

July 2004

Hsinchu, Taiwan, Republic of China

中華民國九十三年七月

# 對稱式光柵耦合器之寬頻研究

研究生：曾凱悌

指導教授：彭松村博士

黃瑞彬博士

國立交通大學

電信工程學系碩士班



光柵最常用的功能除了將入射波的能量耦合至介質波導中之外，還能將介質波導中的表面波轉化成存在於自由空間中的漏波。由於近年來在光學積體電路中耦合元件的需求增加，光柵耦合器扮演著重要的角色。然而，傳統的分析大多著重於在固定頻率條件之下的耦合現象。因此在此文中，我們延續性地論述在寬頻操作的分析之下，對於多種對稱式的光柵耦合器探討其出射光的光束寬度，將在  $1\mu\text{m}$  到  $2\mu\text{m}$  的波帶上維持的一平坦趨勢。之所以選擇對稱形式的光柵，是由於該對稱形狀，將抑制第二諧振的激發，因此在原本應該出現第二空間諧振 ( $n=-2$ ) 的波長處，其能量並沒有如預期般的被激發出來，其光束寬度的寬頻表現也不會因而受到破壞。我們並更深一步地討論，在不同形狀的光柵中，此一波帶在寬頻操作下平坦度的變化。我們發現，正規矩型式 ( $d_1/d = d_2/d = 0.5$ ) 的光柵耦合器，如預期地表現出最小平坦度差異，而三角式光柵則顯示出差異性較大之特性。

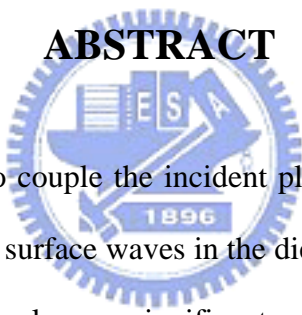
# Clarification of Wideband Grating Couplers with Symmetrical Profiles

**Student: Kai-Ti Tseng**

**Advisor: Dr. Song-Tsuen Peng  
Dr. Ruey-Bing Hwang**

**Department of Communication Engineering  
National Chiao Tung University**

## ABSTRACT

The logo of National Chiao Tung University is a circular emblem with a gear-like border. Inside the circle, there is a stylized building and the letters 'ES' and 'A'. Below the building, the year '1896' is inscribed.

The function of gratings is to couple the incident plane wave energy into the dielectric waveguide or to change the bound surface waves in the dielectric waveguide into leaky waves in free space, and this structure plays a significant role nowadays since the interfacial elements between optical integrated circuits is required urgently. However, the conventional analysis examines the coupling behavior at a fixed value of wavelength. This work, thereby, presents an extended analytical approach to the outgoing beam width on broadband operation, and reveals these properties are remained nearly constant over a wavelength band from  $1\mu\text{m}$  to  $2\mu\text{m}$ . The reason for choosing the symmetric structure is that symmetrical grating avoids excitation of the second ( $n = -2$ ) space harmonic and therefore, the behavior of broadband would not be deteriorated. Moreover, we find the canonic rectangular ( $d_1/d = d_2/d = 0.5$ ) gratings exhibit the smallest difference of flatness, but the symmetric triangular ones, however, present larger variation.

# *Acknowledgement*

*To my advisers, Prof. Peng and Hwang,*



*my lovely lab-mates,*

*&*

*my parents.*

# Contents

---

<b>I</b>	<b>Introduction</b>	<b>1</b>
<b>II</b>	<b>Method of Analysis</b>	<b>3</b>
2.1	FLOQUET'S THEOREM	3
2.2	STATEMENT OF PROBLEM AND BACKGROUND INFORMATION	5
2.3	SMALL PERTURBATION METHOD WITH GREEN'S FUNCTION TECHNIQUE	10
2.3.1	The surface waves guided in the unperturbed structure	12
2.3.2	The leaky waves excited in the perturbed structure	17
2.3.3	Green's function technique	20
<b>III</b>	<b>Numerical results and Discussions</b>	<b>23</b>
3.1	DEPENDENCE OF COUPLING PROPERTIES ON $t_g$ IN DIFFERENT GRATING PROFILES	23
3.2	CHARACTERISTICS OF THE BEAMWIDTH AT BROADBAND OPERATION	30
3.3	DISCUSSION ON VARIATION OF THE BEAMWIDTH ON $\Delta\lambda$ FOR DIFFERENT PROFILE	43
<b>IV</b>	<b>Conclusion</b>	<b>46</b>
	<b>Bibliography</b>	<b>48</b>

# List of Figures

---

Figure 1- 1 Grating coupler components for optical integrated circuits .....	1
Figure 2- 1 Illustration of a basic output coupler which converts surface waves to leaky-wave outgoing beams with angles $\theta^{(n)}$ and beam widths $W^{(n)}$ .....	6
Figure 2- 2 The proper range for the variation of wavelength $\lambda$ versus corresponding effective refraction index $N$ while the central wavelength $\lambda_0=1550$ nm with the period $d=\lambda_0/2$ , $\varepsilon_s=2.3$ .....	8
Figure 2- 3 Geometry of grating structures profile: (a) canonic rectangular type, (b) symmetric triangular type .....	9
Figure 2- 4 General basic multilayer configuration .....	13
Figure 2- 5 The dispersion relation for four-layer TE modes with the following parameters: $N_a=1, N_{gu}=1.41, N_f=1.732, N_s=1.517$ .....	16
Figure 2- 6 Equivalent source-excited transmission-line for perturbed-layer structure .....	19
Figure 3- 1 Types of symmetrical grating profile: (a) rectangular, (b) symmetric triangular, (c) regular trapezoidal and (d) inverted trapezoidal type .....	24
Figure 3- 2(a) Variation of normalized leakage $\alpha\lambda$ versus $t_g/\lambda$ for the TE <sub>0</sub> mode in symmetric gratings with the corrugated ratio of $d_1 = 1$ .....	25
Figure 3- 2(b) Variation of normalized leakage $\alpha\lambda$ versus $t_g/\lambda$ for the TE <sub>0</sub> mode in symmetric gratings with the corrugated ratio of $d_1 = 0.75$ .....	26
Figure 3- 2(c) Variation of normalized leakage $\alpha\lambda$ versus $t_g/\lambda$ for the TE <sub>0</sub> mode in symmetric gratings with the corrugated ratio of $d_1 = 0.5$ .....	27
Figure 3- 2(d) Variation of normalized leakage $\alpha\lambda$ versus $t_g/\lambda$ for the TE <sub>0</sub> mode in symmetric gratings with the corrugated ratio of $d_1 = 0.25$ .....	28
Figure 3- 3 Typical variation of the leakage $\alpha$ versus the height $t_g$ in a rectangular dielectric grating .....	29
Figure 3- 4(a) Variation of $W_{a,-1}/\lambda$ versus $\lambda$ at points P, Q, and R for rectangular grating with aspect ratio symmetric triangular gratings $d_1/d = 0.75$ and $d_2/d = 0.75$ .....	33
Figure 3- 4(b) Variation of $W_{a,-1}/\lambda$ versus $\lambda$ at points P, Q, and R for rectangular grating with	

aspect ratio symmetric triangular gratings $d_1/d = 0.5$ and $d_2/d = 0.5$ .....	33
Figure 3- 4(c) Variation of $W_{a,-1}/\lambda$ versus $\lambda$ at points P, Q, and R for rectangular grating with aspect ratio symmetric triangular gratings $d_1/d = 0.25$ and $d_2/d = 0.25$ .....	34
Figure 3- 5(a) Variation of $W_{a,-1}/\lambda$ versus $\lambda$ at points P, Q, and R for rectangular grating with aspect ratio symmetric triangular gratings $d_1/d = 1$ and $d_2/d = 0$ .....	35
Figure 3- 5(b) Variation of $W_{a,-1}/\lambda$ versus $\lambda$ at points P, Q, and R for rectangular grating with aspect ratio symmetric triangular gratings $d_1/d = 0.75$ and $d_2/d = 0$ .....	35
Figure 3- 5(b) Variation of $W_{a,-1}/\lambda$ versus $\lambda$ at points P, Q, and R for rectangular grating with aspect ratio symmetric triangular gratings $d_1/d = 0.75$ and $d_2/d = 0$ .....	35
Figure 3- 5(c) Variation of $W_{a,-1}/\lambda$ versus $\lambda$ at points P, Q, and R for rectangular grating with aspect ratio symmetric triangular gratings $d_1/d = 0.5$ and $d_2/d = 0$ .....	36
Figure 3- 5(b) Variation of $W_{a,-1}/\lambda$ versus $\lambda$ at points P, Q, and R for rectangular grating with aspect ratio symmetric triangular gratings $d_1/d = 0.75$ and $d_2/d = 0$ .....	35
Figure 3- 5(d) Variation of $W_{a,-1}/\lambda$ versus $\lambda$ at points P, Q, and R for rectangular grating with aspect ratio symmetric triangular gratings $d_1/d = 0.25$ and $d_2/d = 0$ .....	36
Figure 3- 6(a.1) Variation of $W_{a,-1}/\lambda$ versus $\lambda$ at points P, Q, and R for rectangular grating with aspect ratio symmetric triangular gratings $d_1/d = 1$ and $d_2/d = 0.75$ .....	37
Figure 3- 6(a.2) Variation of $W_{a,-1}/\lambda$ versus $\lambda$ at points P, Q, and R for rectangular grating with aspect ratio symmetric triangular gratings $d_1/d = 1$ and $d_2/d = 0.5$ .....	37
Figure 3- 6(a.3) Variation of $W_{a,-1}/\lambda$ versus $\lambda$ at points P, Q, and R for rectangular grating with aspect ratio symmetric triangular gratings $d_1/d = 1$ and $d_2/d = 0.25$ .....	38
Figure 3- 6(b.1) Variation of $W_{a,-1}/\lambda$ versus $\lambda$ at points P, Q, and R for rectangular grating with aspect ratio symmetric triangular gratings $d_1/d = 0.75$ and $d_2/d = 0.5$ .....	38
Figure 3- 6(b.2) Variation of $W_{a,-1}/\lambda$ versus $\lambda$ at points P, Q, and R for rectangular grating with aspect ratio symmetric triangular gratings $d_1/d = 0.75$ and $d_2/d = 0.25$ .....	39
Figure 3- 6(c) Variation of $W_{a,-1}/\lambda$ versus $\lambda$ at points P, Q, and R for rectangular grating with aspect ratio symmetric triangular gratings $d_1/d = 0.5$ and $d_2/d = 0.25$ .....	39
Figure 3- 7(a) Variation of $W_{a,-1}/\lambda$ versus $\lambda$ at points P, Q, and R for rectangular grating with aspect ratio symmetric triangular gratings $d_1/d = 0.75$ and $d_2/d = 1$ .....	40
Figure 3- 7(b.1) Variation of $W_{a,-1}/\lambda$ versus $\lambda$ at points P, Q, and R for rectangular grating with	



aspect ratio symmetric triangular gratings $d_1/d = 0.5$ and $d_2/d = 1$ .....	40
Figure 3- 7(b.2) Variation of $W_{a,-1}/\lambda$ versus $\lambda$ at points P, Q, and R for rectangular grating with aspect ratio symmetric triangular gratings $d_1/d = 0.5$ and $d_2/d = 0.75$ .....	41
Figure 3- 7(c.1) Variation of $W_{a,-1}/\lambda$ versus $\lambda$ at points P, Q, and R for rectangular grating with aspect ratio symmetric triangular gratings $d_1/d = 0.25$ and $d_2/d = 1$ .....	41
Figure 3- 7(c.2) Variation of $W_{a,-1}/\lambda$ versus $\lambda$ at points P, Q, and R for rectangular grating with aspect ratio symmetric triangular gratings $d_1/d = 0.25$ and $d_2/d = 0.75$ .....	42
Figure 3- 7(c.3) Variation of $W_{a,-1}/\lambda$ versus $\lambda$ at points P, Q, and R for rectangular grating with aspect ratio symmetric triangular gratings $d_1/d = 0.25$ and $d_2/d = 0.5$ .....	42
Figure 3- 8 Typical variation of the normalized beamwidth $W/\lambda$ versus wavelength .....	43



# List of tables

---

Table 2- 1 The field components and transmission line parameters of unperturbed structure -----	12
Table 2- 2 The field components and transmission line parameters of perturbed structure -----	18
Table 3- 1 Position of broadband operation point. The center wavelength $\lambda_0$ herein is chosen as 1550 nm -----	31
Table 3- 2(a) $\Delta$ and $\Delta W / W_{Max}$ in rectangular gratings -----	44
Table 3- 2(b) $\Delta$ and $\Delta W / W_{Max}$ in symmetric triangular gratings -----	44
Table 3- 2(c) $\Delta$ and $\Delta W / W_{Max}$ in regular trapezoidal gratings -----	44
Table 3- 2(d) $\Delta$ and $\Delta W / W_{Max}$ in inverse trapezoidal gratings -----	44



# Chapter I

## Introduction

---

Fine periodic structures such as gratings, implemented on an optical waveguide, are widely used as one of the most important elements for optical integrated circuits (OICs) construction. The understanding of the input or output thin-film dielectric grating couplers has been developed well for years. Figure 1-1 illustrates examples of grating couplers for integrated optics and they would change the direction of light as we observe. However, conventional analysis examines their coupling behavior at a fixed value of frequency/wavelength and emphasizes primarily the applications for a narrow wavelength band like frequency-selective devices. Nowadays, the operation over a wide wavelength band, such as spectrum analyzers, broadband fiber communication, and other applications, is more often seen than before. Meanwhile, the wideband laser system applies for the properties of

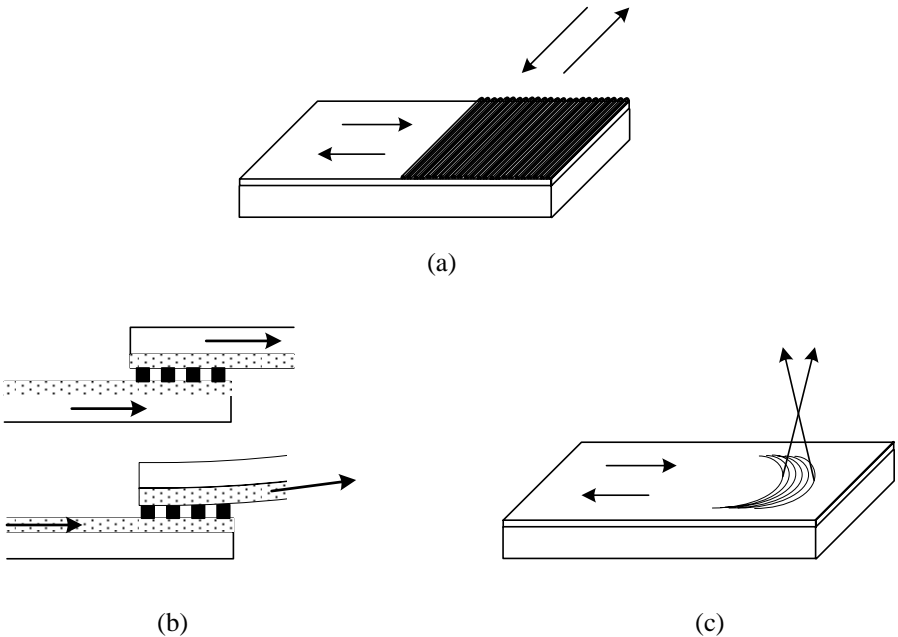


Figure 1- 1 Grating coupler components for optical integrated circuits. (a) Input/output coupler. (b) Waveguide couplers. (c) Focusing coupler.

broader wavelength band as well. This work, therefore, presents the flatness behaviors of grating couplers with the beamwidth over a certain wavelength interval and furthermore provides a simple design procedure for broadband operation.

The following Chapter II is concerned with the method of analysis. The small perturbation method (SPM) is adopted here due to its simplicity of formulations and acceptable accuracy. Electromagnetic fields with a grating layer can be represented as distributed current and/or voltage sources within the transverse transmission-line network in the viewpoint of SPM, and thus a designer applies this method for acquisition of grating parameters.

Subsequently, the results of broadband behavior are explored and discussed in Chapter III, and we then observe the broadband coupling is realizable. While verifying the broadband properties of different types of grating profile, we find these behaviors at certain choices of  $t_g$  remaining flat over a wavelength band from  $1\mu\text{m}$  to  $2\mu\text{m}$  with the central wavelength  $\lambda_0 = 1550\text{ nm}$ . Previous literature [7] has shown that, the curves of leakage factor  $\alpha$  versus the grating height  $t_g$  can be roughly divided into the parabolic region and the bounded fluctuation region. In this work, we show the flatness appearance in the broadband operation region which is posited in the transition between those two regimes mentioned above. Also, a simple flatness criterion for determining parameters for gratings and discussion is then provided at the end of this chapter.

In Chapter IV, we summarize the conditions that a grating coupler is used on broadband operation and comment on the application of SPM approach to other related problems in the conclusion. In addition, the further work in grating couplers is mentioned as well.

# Chapter II

## Method of Analysis

---

### 2.1 FLOQUET'S THEOREM

### 2.2 STATEMENT OF THE PROBLEM AND BACKGROUND INFORMATION

### 2.3 SMALL PERTURBATION METHOD WITH GREEN'S FUNCTION TECHNIQUE

---

#### 2.1 Floquet's Theorem

The traveling waves guided in an axially periodic structure can be sufficiently represented from Floquet's theorem. This theorem, has carried out by Bloch, generalizes a linear ordinary differential equation with periodic coefficients from a linear partial differential equation so as to solve Schrödinger's equation, which is in connection with the propagation of electron waves in large but finite crystals. Consider a wave propagating in infinite periodic structures which periodical direction is along  $\hat{x}$  axis. It is obviously true that the fields along  $x$  differ from the other one at a period  $d$  away by a complex number due to the infinity of periodicity. This complex constant can be separated to real and imaginary part, and they are so-called attenuation coefficients and phase constants and respectively. For the case of TE mode, this property satisfies the wave equation with the periodically variational permittivity  $\varepsilon_0 \varepsilon_r(x)$  such as

$$\left\{ \frac{d^2}{dx^2} + \varepsilon_0 \left[ \varepsilon_{r0} + \varepsilon_{r1} \cos \left( \frac{2\pi}{d} x \right) \right] k_0^2 \right\} \varphi(x) = 0 \quad (2.1)$$

with

$$\varepsilon_r(x) = \varepsilon_{r0} + \varepsilon_{r1} \cos \left( \frac{2\pi}{d} x \right) \quad (2.2)$$

Here we change  $x+d$  instead of  $x$ , and then obtain

$$\left\{ \frac{d^2}{dx^2} + \varepsilon_0 \left[ \varepsilon_{r0} + \varepsilon_{r1} \cos \left( \frac{2\pi}{d}(x+d) \right) \right] k_0^2 \right\} \varphi(x+d) = 0 \quad (2.3)$$

Since the cosine term in (2.3) is periodical as well,  $\varphi(x+d)$  is also a solution of (2.1).

Note that  $\varphi(x)$  is not a periodic function, i.e.  $\varphi(x) \neq \varphi(x+d)$ .

Therefore, a time-harmonic electromagnetic field function  $\varphi(x)$  and  $\varphi(x+d)$  have the same manner as  $\varphi(x+d)$  and  $\varphi(x+2d)$ . Mathematically, we write them as

$$\frac{\varphi(x+d)}{\varphi(x)} = \frac{\varphi(x+2d)}{\varphi(x+d)} = \frac{\varphi(x+md)}{\varphi[x+(m-1)d]} = C \quad (2.4)$$

where  $C$  is a constant. From the above equation, we obtain  $\varphi(x+md) = C^m \varphi(x)$ . Note that  $C^m$  is generally a complex number mentioned previously. Thus it would be written as  $C = \exp(ik_{x0}d)$ , and the generally complex Floquet wave number  $k_{x0} = \beta_0 + i\alpha$  is referred to as the fundamental propagation constant. Such as array antennas, the phase on each one periodical position differs for one  $k_{x0}d$ . The field possesses the property  $\varphi(x+d) = e^{ik_{x0}d} \varphi(x)$ .

In defining a periodic function  $P(x) = e^{-ik_{x0}x} \varphi(x)$ , it may be expanded in a Fourier series by

$$P(x) = \sum_{n=-\infty}^{\infty} A_n e^{i \frac{2n\pi}{d} x} \quad (2.5)$$

and it results in

$$\begin{aligned} \varphi(x) &= \sum_{n=-\infty}^{\infty} A_n e^{i(k_{x0} + \frac{2n\pi}{d})x} \\ &= \sum_{n=-\infty}^{\infty} A_n e^{ik_{xn}x} \end{aligned} \quad (2.6)$$

with

$$k_{.xn} = k_{.x0} + \frac{2n\pi}{d} = \beta_0 + \frac{2n\pi}{d} + i\alpha, \quad n = 0, \pm 1, \pm 2, \dots \quad (2.7)$$

This Fourier series expansion indicates that the field of a normal mode of an axially periodic structure consists of an infinite series  $A_n \exp(k_{.xn}x)$ , called space harmonic, resembling harmonic representation  $e^{i\omega_n t}$  in time domain. The  $n_{th}$  term in (2.7) is called the  $n_{th}$  space harmonic or Hartree harmonic. The functions  $A_n$  represent the corresponding space harmonic amplitudes, while the wave number  $k_{.x0}$  denotes the fundamental space harmonic propagation constant. According to the convergence properties of the Fourier series, the absolute value of  $A_n$  is significantly decreases as  $|n|$  is approximate to infinity. In general, the singled dominant  $n=0$  harmonic is sufficient to describe the field distribution. Note that the wave may consist of positive-going and negative-going waves due to the sign of harmonic order  $n$ . Using the definition of  $P$ , a periodic function of  $x$  with a period  $d$ , therefore the general solution of Equation (2.1) is of the form  $P = \exp(\pm k_{.x0}x)\varphi(x)$ . That is the particular result of Floquet's theorem and commonly the starting point in solving the problem of periodic structures and the periodic property of  $P$  is given

$$P(x+d) = e^{-k_{.x0}d} e^{-k_{.x0}x} \varphi(x+d) = e^{-k_{.x0}x} \varphi(x) = P(x) \quad (2.8)$$

## 2.2 Statement of the Problem and Background Information

As we introduce in Chapter I, output grating couplers are regarded as surface-wave-to leaky-wave converters. It is assumed herein the light wave propagates to  $+\hat{x}$  direction. The fundamental phase constant  $\beta_0$ , which only exists in the grating region instead of non-grating part, would be very close to the propagation factor  $\beta_{.sw}$  of incident surface wave in the non-grating region as long as the relative permittivity of film waveguide  $\epsilon_f$  is mainly larger than the one of grating layer  $\epsilon_g$ . Furthermore, the attenuation coefficient  $\alpha$  is comparably insignificant to  $\beta_0$ . However, we are interested only in these leaky-waves modes

that appear as perturbations of a surface-wave mode. Then it can be assumed as

$$\beta_0 \approx \beta_{sw} > k_0 = 2\pi/\lambda_0 \quad (2.9)$$

where  $\lambda_0$  is a certain wavelength in air and  $k_0$  is the free space wave number at the corresponding wavelength  $\lambda_0$ .

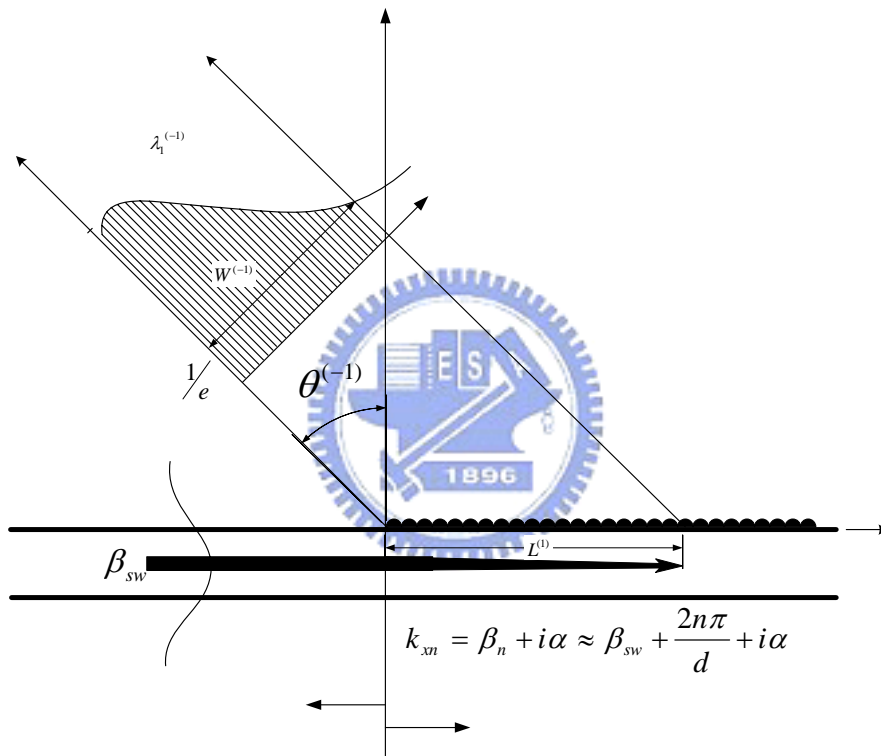


Figure 2- 1 Illustration of a basic output coupler which converts surface waves to leaky-wave outgoing beams with angles  $\theta^{(n)}$  and beam widths  $W^{(n)}$ . Note that both  $\theta^{(n)}$  and  $W^{(n)}$  are functions of wavelength  $\lambda$  of incident surface wave.

The attenuate coefficient  $\alpha$  can be hold as leakage of the energy scattered by a number of diffracted orders after it is assumed that all the materials discussed here are in lossless situations. Due to the diffraction of grating, leaky-wave fields manifest harmonic components with wave numbers  $\beta_n = \beta_0 + 2n\pi/d$  in defining the Equation (2.7), where  $n=0, \pm 1, \pm 2, \dots$  and  $d$  is the period of the grating. Each harmonic corresponding to each



propagating order of grating then scatters outgoingly into the air and substrate material. Figure 2-1 is regarded as a structure that transforms a surface wave into one or more leaky waves. Only the air beam is shown but actually there is similar situation occurring in the substrate. Such a situation is suggested a beam is inclined in the angle  $\theta^{(n)}$  for a certain wavelength  $\lambda_n$ , and the angles would be

$$\theta^{(n)} = \sin^{-1}\left(\frac{\beta_n}{k_0}\right) \quad n = 0, \pm 1, \pm 2, \dots \quad (2.10)$$

Note that the radiation from the grating part occurs only for  $n < 0$  due to the reasonability in Equation (2.10). Practically, the period of grating is appropriately chosen so that a single order harmonic solely propagates, and mostly the  $n = -1$  harmonic is prescribed for design. For minimizing the numbers of outgoing beams to cause only  $n = -1$  harmonic exist in the air and substrate, the period  $d$  must be selected to satisfy

$$|\beta_{-1}/k_0| < N_a \quad \text{and} \quad |\beta_{-2}/k_0| > N_a \quad (2.11)$$

in the air region, and

$$|\beta_{-1}/k_0| < N_s \quad \text{and} \quad |\beta_{-2}/k_0| > N_s \quad (2.12)$$

in the substrate region. The terms  $N_a$  and  $N_s$  denotes the refractive index of air and substrate, and are defined as  $N_a^2 = \varepsilon_a = 1$  and  $N_s^2 = \varepsilon_s$ . The latter terms both in Equation (2.11) and (2.12) imply that the waves do not propagate for all  $n \neq -1$ . Arranging both of equations, we obtain the range of  $N = \beta_0/k_0$  satisfying

$$-1 + \frac{\lambda}{d} < N < 1 + \frac{\lambda}{d} \quad (2.13)$$

and

$$N < \frac{2\lambda}{d} - N_s \quad \text{and} \quad N > N_s - \frac{2\lambda}{d} \quad (2.14)$$

to support the propagating of single harmonic beam. The effective refractive index  $N$  of the thin film waveguide, defined as  $\beta_{sw}/k_0$  or  $\beta_0/k_0$ , increases in a nonlinear way as the operation frequency is increased, and is influenced by the dimension of the structure as well. Figure 2-2 shows the linear programming diagram of the above equations. The forward and backward direction properties of outgoing beams depend on positive and negative values of the angle in Equation (2.10), i.e. it is demarked by the line of  $N = \lambda/d$ . This boundary between these two regions correlates with Bragg reflection condition. Such a resonant situation, however, leads the incident power totally to reflect back to the surface-wave part and that is something to avoid for a designer.

It deserves to be mentioned in Figure 2-2 that a critical point occurs when  $\lambda$  is decreasing to about  $1.25 \mu\text{m}$ . The point indicates the lowest wavelength of the proper operation region. If

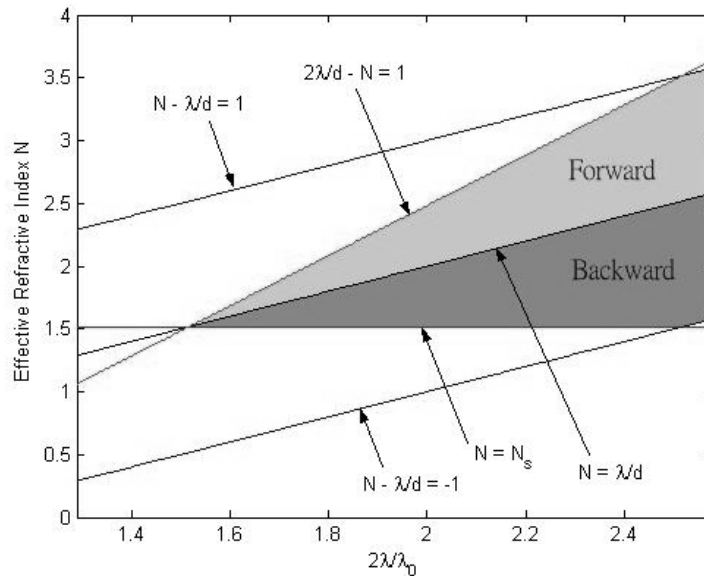


Figure 2- 2 The proper range for the variation of wavelength  $\lambda$  versus corresponding effective refraction index  $N$  while the central wavelength  $\lambda_0=1550 \text{ nm}$  with the period  $d = \lambda_0 / 2$ ,  $\epsilon_s = 2.3$ .

the wavelength is selected to be below this point, the second or higher-order surface modes might be excited. These unwanted beams would cause unnecessary loss and degenerate the broadband performance.

At larger wavelength, the horizontal fraction of the output beam is oriented along  $-\hat{x}$  direction while  $\beta_{-1} < 0$ . As the wavelength is decreasing, the leaky beam rotates clockwise to the normal even to form a forward leaky wave. Here we define  $L$  as the effective coupling length is reciprocal of attenuate coefficient, i.e.  $L \equiv 1/\alpha$ . According to this definition, the effective width of the beam in air is  $W^{(n)} = L^{(n)} \cos\theta^{(n)}$ . This effective width  $W^{(n)}$  depends on the operation wavelength since both of decay factor  $\alpha^{(n)}$  and diffraction angle  $\theta^{(n)}$  are functions of  $\lambda^{(n)}$ .

Typical thin-film grating configuration is shown in Figure 2-2. Subscripts  $a, g, f,$  and  $s$  denote air, grating layer, firm and substrate region respectively. The relative permittivity  $\varepsilon$  of each layer is a pure real number because of the assumption of lossless property in all materials. The thickness of residual layer here is ignored for simplifying the problem. Due to Tamir and Peng's investigation which develops the relation of normalized leakage versus aspect ratio for canonic rectangular grating [7], the aspect ratio in Figure 2-2 (a) is properly chosen as  $1/2$ . This study, however, is focused on the relation between the effective width  $W$ , of outgoing beam in air region with the operation wavelength  $\lambda$ , and henceforth to develop design criteria that minimize the variation of  $W$  as  $\lambda$  varies over a certain larger frequency interval.

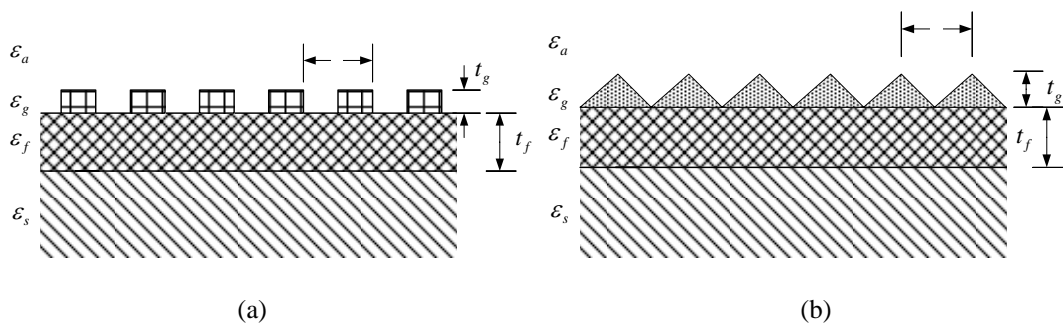
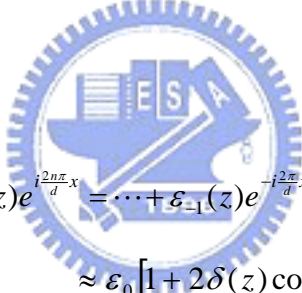


Figure 2- 3 Geometry of grating structures profile: (a) canonic rectangular type, (b) symmetric triangular type

### 2.3 Small Perturbation Method with Green's Function Technique

In this paper, the improved first-order small perturbation method (SPM) is introduced to analyze the plane-wave diffracting and scattering out of the gratings. This approach, was sequentially developed by Handa *et al.*[9], Tamir *et al.*[7], and by Hwang and Wei [13], is much more current than the rigorous method, and its computational application provides the analytical insight for developing design criteria with a short time. In view of SPM, the grating layer is regarded as a perturbed variation on the uniform multilayer. Such a concept leads to translate the boundary value problems and source of a diffraction wave to the transmission-line modal appropriately for periodic dielectric medium.

The infinite dimension of the  $\hat{y}$  direction is assumed in our work, i.e.  $d/dy = 0$ . Due to the periodicity of the grating, the dielectric variation in the grating can be expanded as one-dimension Fourier expansion



$$\begin{aligned}\varepsilon(x, z) &= \sum_{-\infty}^{\infty} \varepsilon_n(z) e^{i\frac{2n\pi}{d}x} = \cdots + \varepsilon_{-1}(z) e^{-i\frac{2\pi}{d}x} + \varepsilon_0 + \varepsilon_1(z) e^{i\frac{2\pi}{d}x} + \cdots \\ &\approx \varepsilon_0 \left[ 1 + 2\delta(z) \cos\left(\frac{2\pi}{d}x\right) \right] \\ &\equiv \varepsilon_u + \varepsilon_p(x, z)\end{aligned}\tag{2.15}$$

where  $\varepsilon_n$  is the corresponding Fourier-series coefficients.  $\varepsilon_p(x, z)$  is considered as a perturbed term imposed on a layer with the dielectric constant which depends on the position  $x$  and  $z$ . The above expression only exists on the grating layer because all the other layers have been assumed uniform, i.e. there is no perturbation inside those layers except grating. The electric and magnetic fields of leaky-wave can be respectively taken apart to corresponding unperturbed and perturbed terms by Fourier series expansion as

$$\mathbf{E} = \mathbf{E}_u + \mathbf{E}_p\tag{2.16}$$

and

$$\mathbf{H} = \mathbf{H}_u + \mathbf{H}_p \quad (2.17)$$

The relation of  $\mathbf{E}_u$  and  $\mathbf{H}_u$  are independent from other perturbed fields, i.e. these two unperturbed fields generate each other but  $\mathbf{E}_p$  and  $\mathbf{H}_p$  while they are introduced in to Maxwell's equations. With the notation, Maxwell's equations can be taken the form

$$\nabla \times (\mathbf{E}_u + \mathbf{E}_p) = i\omega\mu_0(\mathbf{H}_u + \mathbf{H}_p) \quad (2.18)$$

and

$$\begin{aligned} \nabla \times (\mathbf{H}_u + \mathbf{H}_p) &= -i\omega\varepsilon_0[\varepsilon_u + \varepsilon_p(x, z)](\mathbf{E}_u + \mathbf{E}_p) \\ &= -i\omega\varepsilon_0\varepsilon_u\mathbf{E}_u - i\omega\varepsilon_0\varepsilon_p(x, z)\mathbf{E}_u - i\omega\varepsilon_0\varepsilon_u\mathbf{E}_p - i\omega\varepsilon_0\varepsilon_p(x, z)\mathbf{E}_p \end{aligned} \quad (2.19)$$

where  $\varepsilon_0$  and  $\mu_0$  are the permittivity and permeability in vacuum. In Equation (2.19), the unperturbed electric  $\mathbf{E}_u$  is generated merely due to the curl operation of  $\mathbf{H}_u$  by the previous statement, and hence the last three terms can be viewed as fields produced by perturbed magnetic field  $\mathbf{H}_p$ . If the term  $\varepsilon_p\mathbf{E}_p$  has been assumed to be significantly small compared to any other term, thus the perturbed part of Equation (2.19) is given

$$\begin{aligned} \nabla \times \mathbf{H}_p &= -i\omega\varepsilon_0\varepsilon_u\mathbf{E}_p - i\omega\varepsilon_0\varepsilon_p(x, z)\mathbf{E}_u \\ &= -i\omega\varepsilon_0\varepsilon_u\mathbf{E}_p + \mathbf{J}_{\text{eq}}(x, z) \end{aligned} \quad (2.20)$$

with

$$\mathbf{J}_{\text{eq}} \equiv -i\omega\varepsilon_0\varepsilon_p(x, z)\mathbf{E}_u \quad (2.21)$$

	TE modes	TM modes
Field Components	$H_{xu} = -I_u(z) \exp(i\beta_0 x)$ $E_{yu} = V_u(z) \exp(i\beta_0 x)$ $H_{zu} = \frac{\beta_0}{\omega \mu_0} E_{yu}$	$E_{xu} = V_u(z) \exp(i\beta_0 x)$ $H_{yu} = I_u(z) \exp(i\beta_0 x)$ $E_{zu} = -\frac{\beta_0}{\omega \epsilon_0 \epsilon_{gu}} E_{yu}$
Characteristic Admittances	$Y_{qu} = \frac{1}{Z_{qu}} = \frac{k_{qu}}{\omega \mu_0}$	$Y_{qu} = \frac{1}{Z_{qu}} = \frac{\omega \epsilon_0 \epsilon_{qu}}{k_{qu}}$
Propagation Coefficient	$k_{qu} = \sqrt{k_0^2 \epsilon_{qu} - \beta_0^2} = k_0 \sqrt{\epsilon_{qu} - N^2} \quad \text{with} \quad N = \frac{\beta_0}{k_0}$	

Table 2- 1 The field components and transmission line parameters of unperturbed structure.

The accuracy of small perturbation method strongly depends on whether the supposition is held or not. If the term  $\epsilon_p$  is not small enough, the last term of Equation (2.19) can not be ignored and that would cause inaccuracy of analysis. Based on Equation (2.21), the equivalent current source  $\mathbf{J}_{eq}$  is regarded as the generation of spatial variation of medium. Combining with following transmission-line modal, the characteristics of a diffraction phenomenon of a grating coupler is investigated.

### 2.3.1 The surface waves guided in the unperturbed structure

For the uniform two-dimension-multilayer structure, the fields are of TE and TM types. The components of each type can be represented by the equivalent voltages  $V = V(z)$  and the currents  $I = I(z)$  waves traveling along the  $\hat{z}$  direction. Note that the  $\hat{z}$  direction is transverse to the original direction of incident surface waves. As summarized in Table 2-1, those components obey the conventional transmission line equation given by

$$\frac{dV_{qu}(z)}{dz} = ik_{qzu} Z_{qu} I_{qu}(z) \quad (2.22)$$

$$\frac{dI_{qu}(z)}{dz} = ik_{qzu} Y_{qu} V_{qu}(z) \quad (2.23)$$

where  $q$  denotes  $a, g, f$  and  $s$  respectively and the subscription  $u$  exhibits the unperturbed quantities. Because the relative dielectric constants in all materials  $\epsilon_{qu}$  are all real numbers, the propagation constants are either real or imaginary numbers. We note that two of these factors  $k_{azu}$  and  $k_{szu}$  are purely imaginary since the fields of surface waves evanesce in the two layers and  $k_{fzu}$  is reversely real because the wave sinusoidally propagates in the firm in Figure 2-4.

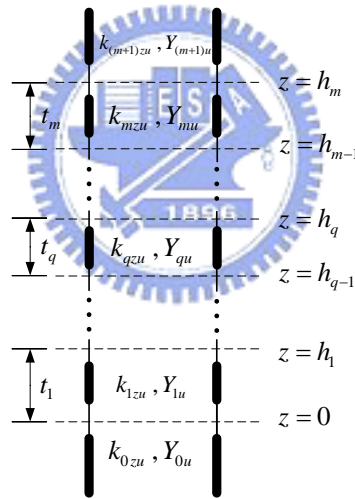


Figure 2- 4 General basic multilayer configuration.

For dealing with different geometric types of grating or the structures with many layers, the general basic grating configuration is introduced here. Assume that the transmission-line model for  $(m+1)$  layers is shown as Figure 2-4. From the transmission-line theory, the field is initially defined in the terminal layers such as

$$V_{0u} = C_0 \exp(-ik_{0zu} z) \quad (2.24)$$

$$V_{(m+1)u} = C_{(m+1)} \exp(-ik_{(m+1)zu} (z - h_m)) \quad (2.25)$$

With the consistency relation

$$1 - \Gamma_{qu}^+ \Gamma_{qu}^- \exp(i2k_{qzu} t_q) = 0 \quad (2.26)$$

where the terms  $\Gamma_{qu}^+$  and  $\Gamma_{qu}^-$  is regarded as the reflection coefficients looking into the upper and lower boundaries of the  $q$  medium, one then find that the representation of fields would be

$$V_{qu} = C_q \left[ \exp(ik_{qzu} (z - h_{q-1})) + \Gamma_{qu}^+ \exp(i2k_{qzu} t_q) \exp(-ik_{qzu} (z - h_{q-1})) \right] \quad (2.27)$$

while  $q \neq 0$  or  $q \neq (m+1)$ . In Equation (2.27), the reflection coefficient  $\Gamma_{qu}^+$  is given by

the reflectance relations



$$\Gamma_{1u}^- = \frac{Y_{1u} - Y_{0u}}{Y_{1u} + Y_{0u}} \quad (2.28)$$

$$\Gamma_{mu}^+ = \frac{Y_{mu} - Y_{(m+1)u}}{Y_{mu} + Y_{(m+1)u}} \quad (2.29)$$

Thus the reflection coefficients looking into the upward and downward to boundaries of the  $q$  medium are

$$\Gamma_{qu}^+ = \frac{(Y_{qu} - Y_{[q+1],u}) + (Y_{qu} + Y_{[q+1],u}) \Gamma_{[q+1],u}^+ e^{i2k_{(q+1),u} t_{(q+1)}}}{(Y_{qu} + Y_{[q+1],u}) + (Y_{qu} - Y_{[q+1],u}) \Gamma_{[q+1],u}^+ e^{i2k_{(q+1),u} t_{(q+1)}}} \quad (2.30)$$

and

$$\Gamma_{qu}^- = \frac{(Y_{qu} - Y_{[q-1],u}) + (Y_{qu} + Y_{[q-1],u}) \Gamma_{[q-1],u}^- e^{i2k_{(q-1),u} t_{(q-1)}}}{(Y_{qu} + Y_{[q-1],u}) + (Y_{qu} - Y_{[q-1],u}) \Gamma_{[q-1],u}^- e^{i2k_{(q-1),u} t_{(q-1)}}} \quad (2.31)$$



while  $q \neq 0$  or  $q \neq (m+1)$  as well as the field representations. The constant coefficients  $C_0$ ,  $C_{(m+1)}$ , and  $C_q$  satisfy the continuity between two distinct layers of materials. For normalizing with convenience, i.e.  $C_l = 1$ , other coefficients would be given by

$$C_0 = 1 + \Gamma_{1u}^+ e^{i2k_{1z}t_1} \quad (2.32)$$

and

$$C_q = \frac{C_{q-1} e^{i2k_{(q-1),u}t_{(q-1)}} (1 + \Gamma_{(q-1),u}^+)}{1 + \Gamma_{qu}^+ e^{i2k_{qu}t_q}} \quad (2.33)$$

The dispersion relation  $\beta_0(\lambda)$  for the surface wave modes in the uniform multilayer is found by using many of well-developed methods, such as a transverse-resonance technique as following. This technique is based on the fact that in a waveguide at cutoff, the fields form standing waves in the transverse plane of the waveguide. An equivalent transmission-line network of the four-layer configuration with respect to the transverse  $\hat{z}$  is modified in Figure 2.4. Consequently all of the modes are obtained by solving the eigenvalue equation in the form

$$Z_{up}(z) + Z_{dn}(z) = 0 \quad \text{for all } z \quad (2.34)$$

where  $Z_{up}$  and  $Z_{dn}$  are the input impedance looking up and down, respectively, and they are given by

$$Z_{up}(z) = Z_{gzu} \frac{Z_{azu} - iZ_{gzu} \tan(k_{gzu} t_g)}{Z_{gzu} - iZ_{azu} \tan(k_{gzu} t_g)} \quad (2.35)$$

$$Z_{dn}(z) = Z_{fzu} \frac{Z_{szu} - iZ_{fzu} \tan(k_{fzu} t_f)}{Z_{fzu} - iZ_{szu} \tan(k_{fzu} t_f)} \quad (2.36)$$

where  $k_{qzu}$  and  $Z_{qzu}$  are the propagation constants and characteristics impedances on Table 2.1. Hence the effective refractive index  $N(\lambda) = \beta_0(\lambda) / k_0$  for any given  $\lambda$  is determined as shown in Figure 2-7. Note that the assumption of Equation (2.9) is established while the thickness of grating approximates to zero since the relative dielectric constant of grating  $\epsilon_{gu}$ , in general, is equal to neither  $\epsilon_s$  nor  $\epsilon_f$ . Hence the result of dispersion is restricted to the structure which has small  $t_g$  in comparison with  $t_f$ .

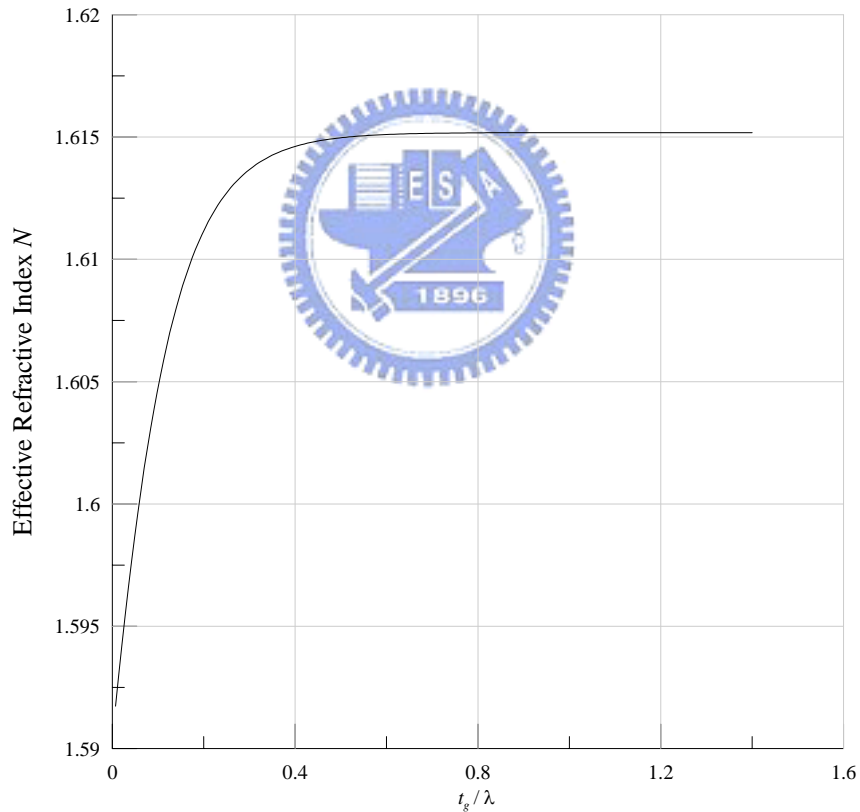


Figure 2- 5 The dispersion relation for four-layer TE modes with the following parameters:

$$N_a=1, N_{gu}=1.41, N_f=1.732, N_s=1.517.$$

The total power guided in the form of the surface-wave can be obtain by integrating corresponding 2-D Poynting vector. Here the appropriate expressions fields are selected from Table 2-1. Finally we find

$$P = \int_{-\infty}^{\infty} (\mathbf{E}_u \times \mathbf{H}_u^*) \cdot \hat{x} dz \quad (2.37)$$

This term would help for estimating the leakage of power in the form of leaky-wave.

### 2.3.2 The leaky waves excited in the perturbed structure

In the previous section, the phenomenon of the unperturbed structure is described. Here it is assumed that the electric field of the incident plane-wave is in the  $\hat{y}$  direction, i.e. TE mode. To obtain the leaky-wave fields, we choose the space harmonic representations in Table 2.2. With the Equation (2.21), the  $n_{th}$  set of the space harmonic amplitude satisfies the source-excited transmission-line relations as shown in Equation (2.38) and (2.39). In these two equations, the distributed voltages  $v_n(z)$  and currents  $i_n(z)$  are generated by the perturbing periodicity and only occur in the region of grating.

$$\frac{dV_{qn}}{dz} = ik_{qzn} Z_{qn} I_{qn} - v_n \quad (2.38)$$

$$\frac{dI_{qn}}{dz} = ik_{qzn} Y_{qn} I_{qn} - j_n \quad (2.39)$$

Since the distributed sources only exist in the grating layer, the corresponding boundary conditions of the impedances at the grating terminal looking upward and downward with the above two equations are given by

$$\left\{ i\omega\mu_0 \frac{V_n(z)}{\partial V_n(z) / \partial z} \right\}_{z=0} = Z'_{fn} \quad (2.40)$$

$$\text{and} \quad \left\{ i\omega\mu_0 \frac{V_n(z)}{\partial V_n(z) / \partial z} \right\}_{z=t_g} = Z_{an} \quad (2.41)$$

	TE modes	TM modes
Field Components	$H_{xp} = -\sum_n I_n(z) \exp(i\beta_n x)$ $E_{yp} = \sum_n V_n(z) \exp(i\beta_n x)$	$E_{xp} = \sum_n V_n(z) \exp(i\beta_n x)$ $H_{yp} = \sum_n I_n(z) \exp(i\beta_n x)$
Characteristic Admittances	$Y_{qn} = \frac{1}{Z_{qn}} = \frac{k_{qzn}}{\omega\mu_0}$	$Y_{qn} = \frac{1}{Z_{qn}} = \frac{\omega\epsilon_0\epsilon_{qu}}{k_{qzn}}$
Equivalent Source	$v_n = 0$ $j_n = -i\omega\epsilon_0\epsilon_n(z)V_u(z)$	$v_n = -i\frac{\beta_0\beta_n\epsilon_n(z)}{\omega\epsilon_0\epsilon_{gu}}I_u(z)$ $j_n = -i\omega\epsilon_0\epsilon_n(z)V_u(z)$
Propagation Coefficient	$k_{qzn} = \sqrt{k_0^2\epsilon_{qu} - \beta_n^2} = k_0\sqrt{\epsilon_{qu} - \left(N + n\frac{\lambda}{d}\right)^2}$	

Table 2- 2 The field components and transmission line parameters of perturbed structure.

The analogous representations of parameters are known in Figure 2-6. For TE mode, the effect of grating dielectric perturbation is viewed as current-excited sources. From Equation (2.38) and (2.39), a second-order differential equation, as shown in the following, is then derived

$$\left(\frac{d^2}{dz^2} + k_{qzn}^2\right)V_n(z) = -i\omega\mu_0 j_n(z) \quad (2.42)$$

With the boundary conditions shown in (2.40) and (2.41), the voltage distribution along the  $\hat{z}$  direction in the grating layer is given by

$$V_n(z) = -i\omega\mu_0 \int_0^{t_g} G_n(z|z') j_n(z') dz' \quad (2.43)$$

where  $G_n(z|z')$  is the Green's function that introduces the unit amplitude generators of voltage and current to represent the excitations  $V_n(z)$  employed in Figure 2-6 and its mathematical derivation is detailed in the next section.

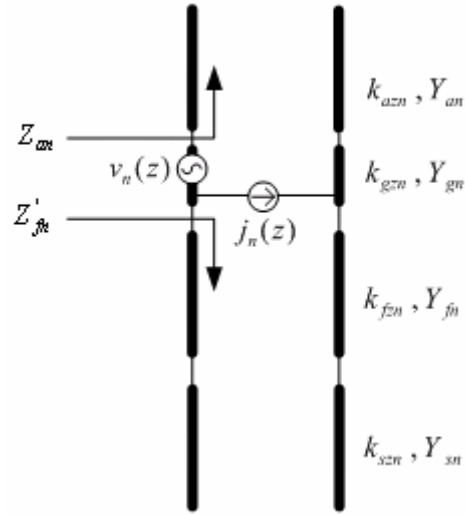


Figure 2- 6 Equivalent source-excited transmission-line for perturbed-layer structure.

The leakage parameter  $\alpha$  of the leaky-wave field is obtained by recalling that the power  $P(x)$  in Equation (2.37) along the perturbed structure varying as  $\exp(-2\alpha x)$  would satisfy

$$\frac{dP}{dx} = -2\alpha P \quad (2.44)$$

where the change in power  $P$  occurs longitudinally since the harmonic components of leaky waves radiate to air or substrate. Thus rate of change of  $P$  in Equation (2.44) can be also written as

$$\begin{aligned} -\frac{dP}{dx} &= P_{rad} = \sum_m P_{am} + \sum_n P_{sn} \\ &= \sum_m |V_{am}|^2 \Re\{Y_{am}\} + \sum_n |V_{sn}|^2 \Re\{Y_{sn}\} \end{aligned} \quad (2.45)$$

The subscripts  $n$  and  $m$  denote the corresponding order of harmonics in air region and

substrate region respectively. While leaking away from the film layer, the total power per unit length  $p_{rad}$  then equal to the summation of all the harmonic power per unit length of the respective regions. Combining Equation (2.44) and (2.45), we get

$$\begin{aligned}\alpha &= \sum_m \alpha_{am} + \sum_n \alpha_{sn} \\ &= \frac{p_{rad}}{2P} = \frac{1}{2P} \left\{ \sum_m p_{am} + \sum_n p_{sn} \right\}\end{aligned}\quad (2.46)$$

where the  $m_{th}$  or  $n_{th}$  harmonic of power per unit length  $p_{am}$  or  $p_{sn}$  involves a copious algebraic derivation with Green's function.

The other significant factor for design of grating couplers is the efficiency of power coupling  $\eta_{ql}$  where  $q$  can be as  $a$  or  $s$  to represent the proportion of power radiated away to air or substrate region and  $l$  denotes the relative harmonics. Consequently the efficiency can be defined

$$\eta_{al} \equiv \frac{p_{al}}{p_{rad}} = \frac{|V_{al}|^2 \Re\{Y_{al}\}}{\sum_n |V_{an}|^2 \Re\{Y_{an}\} + \sum_m |V_{sm}|^2 \Re\{Y_{sm}\}}\quad (2.47)$$

Those two terms, leakage parameter and coupling coefficient, exhibit the properties for design criterion to lay the operation points. In this research, we would select some operation points after figuring the former parameter due to the variation on the outgoing beamwidth. In addition, the promotion on power efficiency is often investigated by the structure with asymmetry.

### 2.3.3 Green's function technique

With the configuration in Figure 2-6, the one-dimensional differential equation in Equation (2.42) can be solved by Green's function technique as following

$$\left( \frac{d^2}{dz^2} + k_{gn}^2 \right) G_n(z|z') = \delta(z-z') \quad (2.48)$$

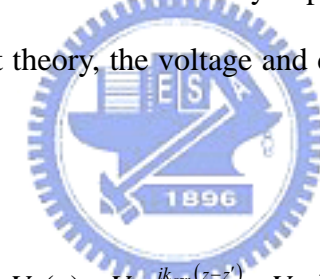
with the boundary conditions,

$$\left\{ i\omega\mu_0 \frac{G_n(z)}{\partial G_n(z)/\partial z} \right\}_{z=0} = Z'_{fn} \quad (2.49)$$

$$\left\{ i\omega\mu_0 \frac{G_n(z)}{\partial G_n(z)/\partial z} \right\}_{z=t_g} = Z_{an} \quad (2.50)$$

where  $\delta(z-z')$  is dirac delta function. This equation presents that the electromagnetic fields radiated by point current excitations are conveniently expressed in terms of Green's function.

According to the classical circuit theory, the voltage and current components due to the point source can be written as



$$V_n(z) = V_+ e^{ik_{gn}(z-z')} + V_- e^{-ik_{gn}(z-z')} \quad (2.51)$$

where  $V_+$  and  $V_-$  are undetermined coefficients corresponding to the magnitudes of the wave traveling upward and downward. While  $z=t_g$ , the relation between these two unknown coefficients would be

$$\frac{V_-}{V_+} = \Gamma_{gan} e^{2ik_{gn}(t_g-z)} \quad (2.52)$$

where the reflection coefficient of for  $n_{th}$  harmonic  $\Gamma_{gan} = (Z_{an} - Z_{gn}) / (Z_{an} + Z_{gn})$ , and thus Equation (2.53) is rewritten as

$$V_n(z = z') = V_+ + V_- = V_+ \left(1 + \Gamma_{gan} e^{2ik_{gan}(t_g - z')}\right) \quad (2.53)$$

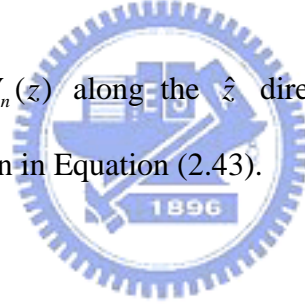
For a point source excited at  $z = z'$ , the following equation would be satisfied

$$V_n(z = z') = 1 \cdot \{Z_n^{up}(z') \parallel Z_n^{dn}(z')\} \quad (2.54)$$

where  $Z_n^{up}(z')$  and  $Z_n^{dn}(z')$  denote the impedances looking upward and downward at the point  $z = z'$ , and  $V_+$ , however, is obtained by the above two equations to acquire the Greens' function such as

$$G_n(z | z') = \frac{e^{ik_{gan}(z-z')} + \Gamma_{gan} e^{-ik_{gan}(z+z'-2t_g)}}{1 + \Gamma_{gan} e^{2ik_{gan}(t_g - z')}} \{Z_n^{up}(z') \parallel Z_n^{dn}(z')\} \quad (2.55)$$

Thus, the voltage distribution  $V_n(z)$  along the  $\hat{z}$  direction in the grating layer will be obtained from the integral equation in Equation (2.43).





# Chapter III

## Numerical Results and Discussions

---

### 3.1 DEPENDENCE OF COUPLING PROPERTIES ON $t_g$ IN DIFFERENT GRATING PROFILES

### 3.2 CHARACTERISTICS OF THE BEAMWIDTH AT BROADBAND OPERATION

### 3.3 DISCUSSION ON VARIATION OF THE BEAMWIDTH ON $\Delta\lambda$ FOR DIFFERENT PROFILE

---

Based on the perturbation approach with Green's function introduced in Chapter II, it is feasible to delve into the interconnection of properties of the power leakage and geometric/material parameters for implementing. However, the detail investigation on their relation has been discussed well by and Stone [8] and Peng [7] in the early year. Due to the strong dependence of the leakage and grating height, here we emphasize on  $t_g$  to generalize the wideband operation design criteria with different symmetrical profiles of gratings.

The reason for the choice of symmetrical structures is the feature avoiding the excitation of higher order harmonics. Recalling the Section 2.2, a second ( $n = -2$ ) order of harmonic begins to propagate at a certain wavelength on the interval  $\Delta\lambda$  that we concern about. The undesired energy deteriorates the stable property on broadband operation and thus the bandwidth is consequently reduced. Nevertheless, the effect of the second order harmonic is invalid in this work since the leaky wave are only excited to the odd order harmonics in case of the symmetrical grating profiles, i.e. only  $n = \pm 1, \pm 3, \pm 5 \dots$  harmonics exist.

Herein, the rectangular, triangular and trapezoidal profiles with symmetry are adopted as show in Figure 3-1. The upper corrugation width  $d_1$  and the lower one  $d_2$  influence upon the leakage parameter  $\alpha$ , which comparably strongly depends on  $t_g$ . As the assumption in Chapter II, only a single order, i.e.  $n = -1$ , is propagating if it is not mentioned particularly. The results are shown in Figure 3-2 for  $\alpha\lambda$  curves as functions of  $t_g/\lambda$  for types which have

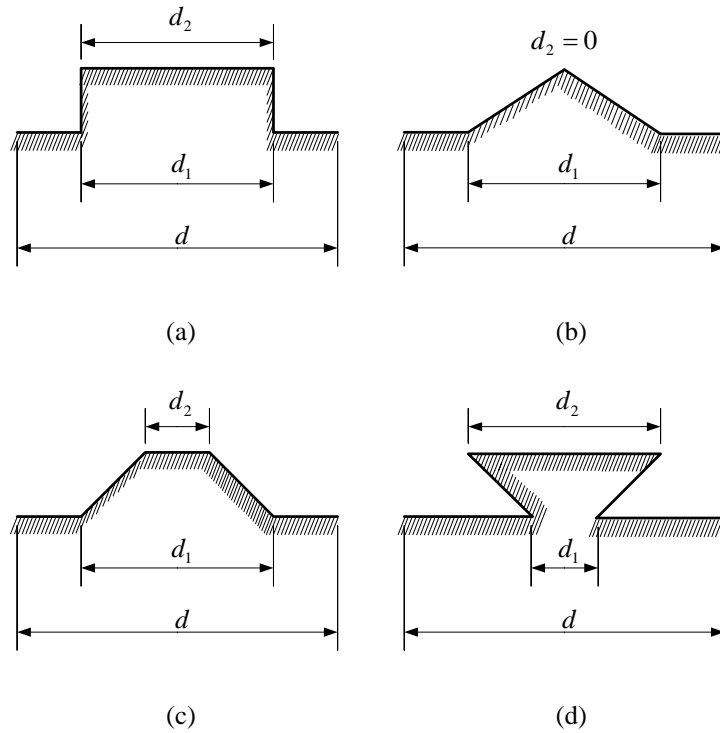


Figure 3- 1 Types of symmetrical grating profile: (a) rectangular, (b) symmetric triangular, (c) regular trapezoidal and (d) inverted trapezoidal type.

the fixed ratios of  $\lambda/d = 0.52$  for  $TE_0$ -mode.

The behavior of  $TM_0$ -mode or other higher mode can be also obtained by the similar method. There just the fundamental  $TE_0$  case is shown here since these expressions give a smaller value of  $\alpha$  for the TM mode than for the TE mode. This is because the electric fields of both guided and leaky mode make a large angle in the TM mode while they are parallel to each other in the TE mode. Moreover, the gratings which consist of isotropic medium do not yield the radiation of polarization differing from that of the guided-mode wave.

Forerunner implicated the preciseness of the approximate perturbation approach generally decreases as  $t_g/\lambda$  in comparison with the rigorous method. In spite of inaccuracy, the larger values of  $t_g/\lambda$  are seldom of practical interesting while the grating is assayed by its broadband behavior. Furthermore, the SPM is adopted with appropriateness in this paper.

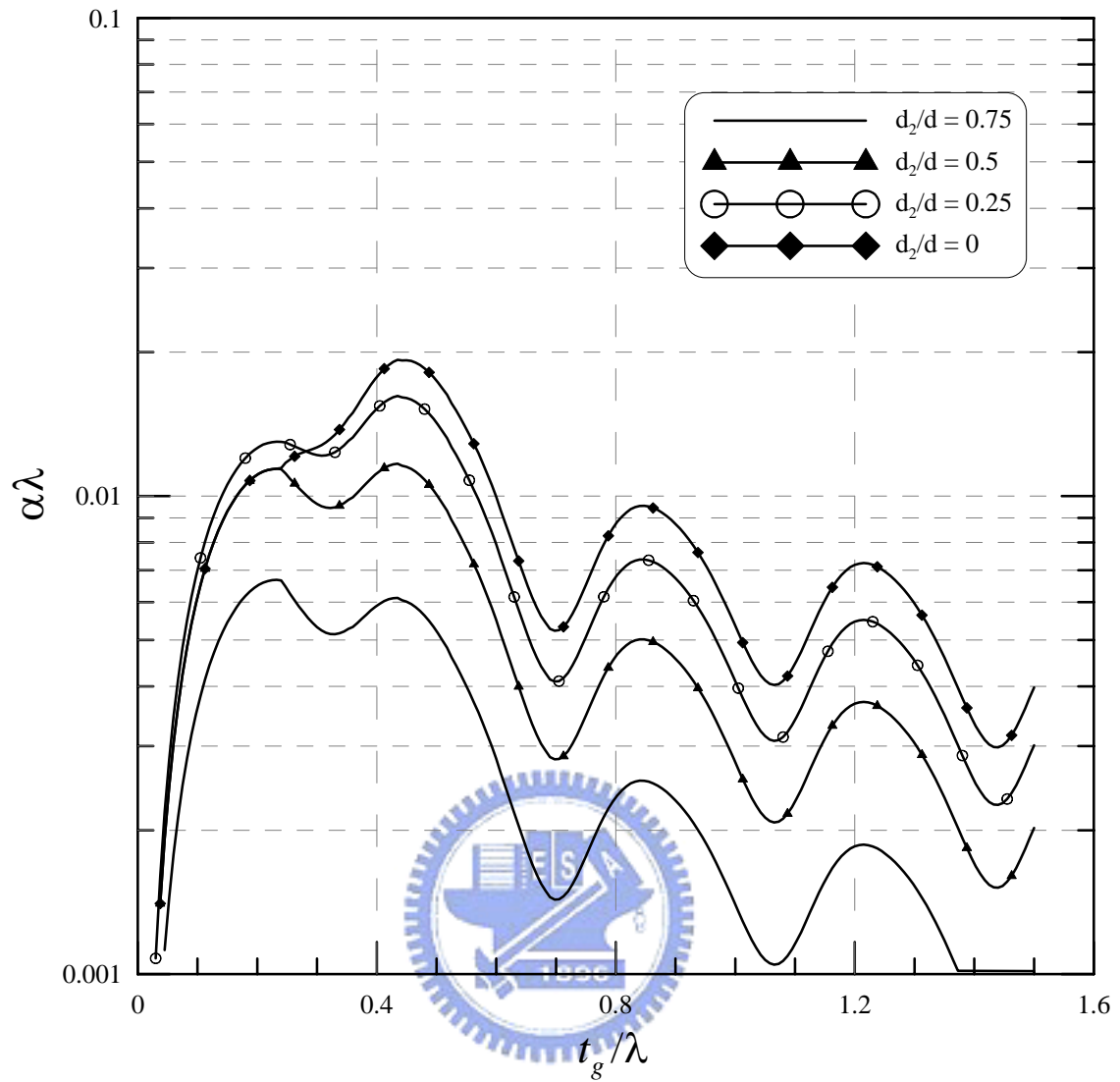


Figure 3- 2(a) Variation of normalized leakage  $\alpha\lambda$  versus  $t_g/\lambda$  for the  $TE_0$  mode in symmetric gratings with the corrugated ratio of  $d_1/d = 1$ .

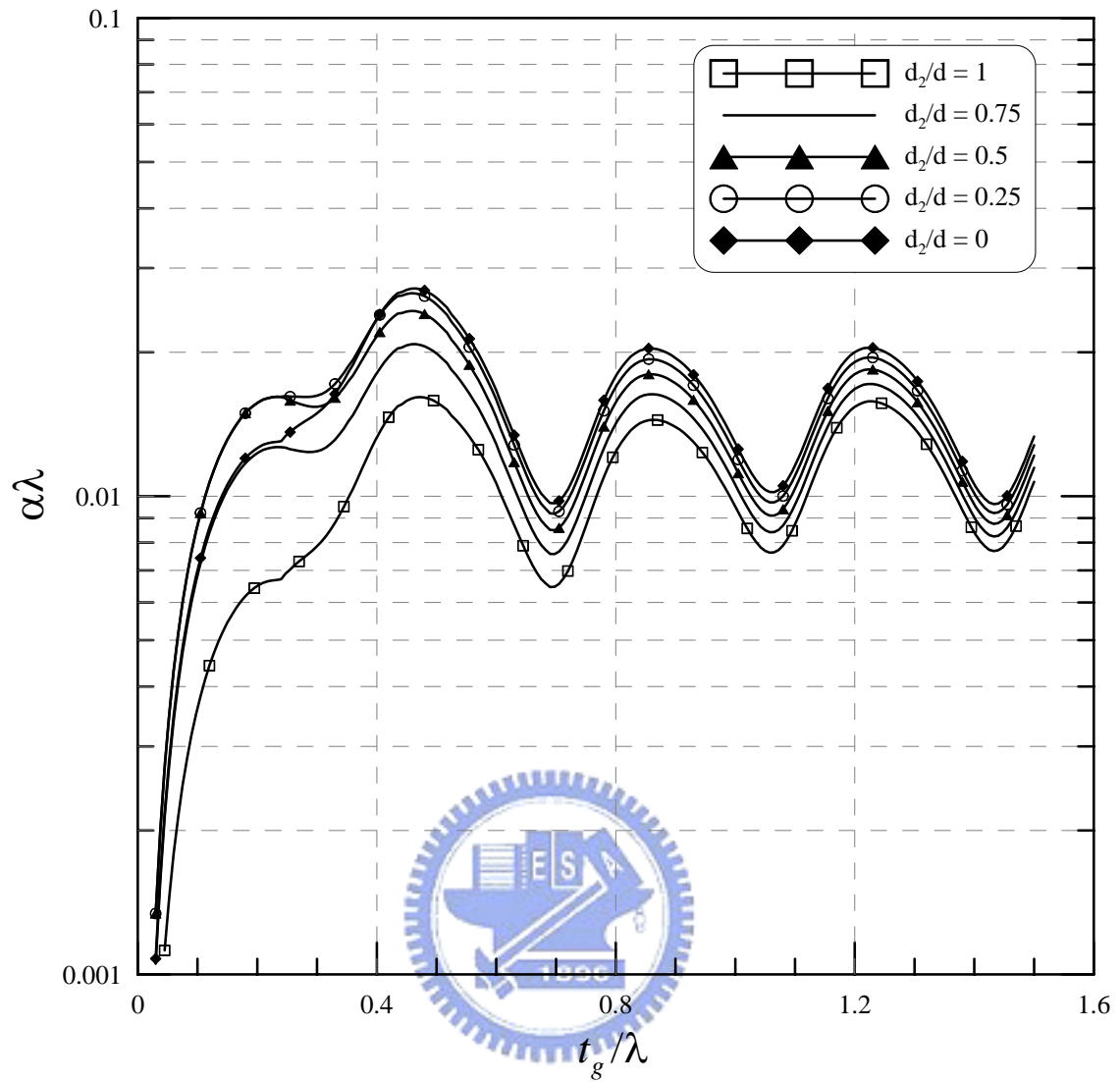


Figure 3-2(b) Variation of normalized leakage  $\alpha\lambda$  versus  $t_g/\lambda$  for the  $TE_0$  mode in symmetric gratings with the corrugated ratio of  $d_1/d = 0.75$ .

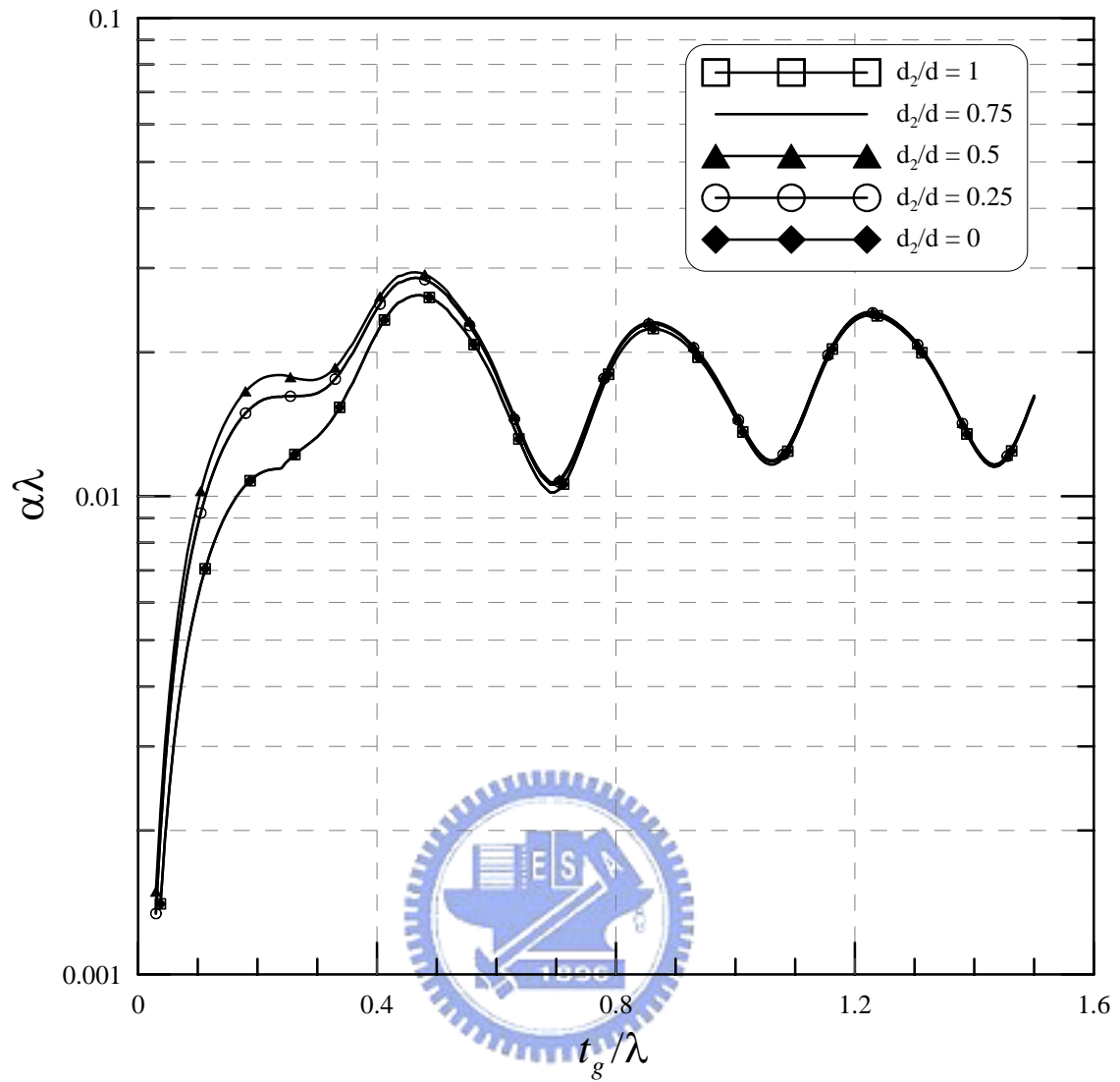


Figure 3-2(c) Variation of normalized leakage  $\alpha\lambda$  versus  $t_g/\lambda$  for the  $TE_0$  mode in symmetric gratings with the corrugated ratio of  $d_1/d = 0.5$ .

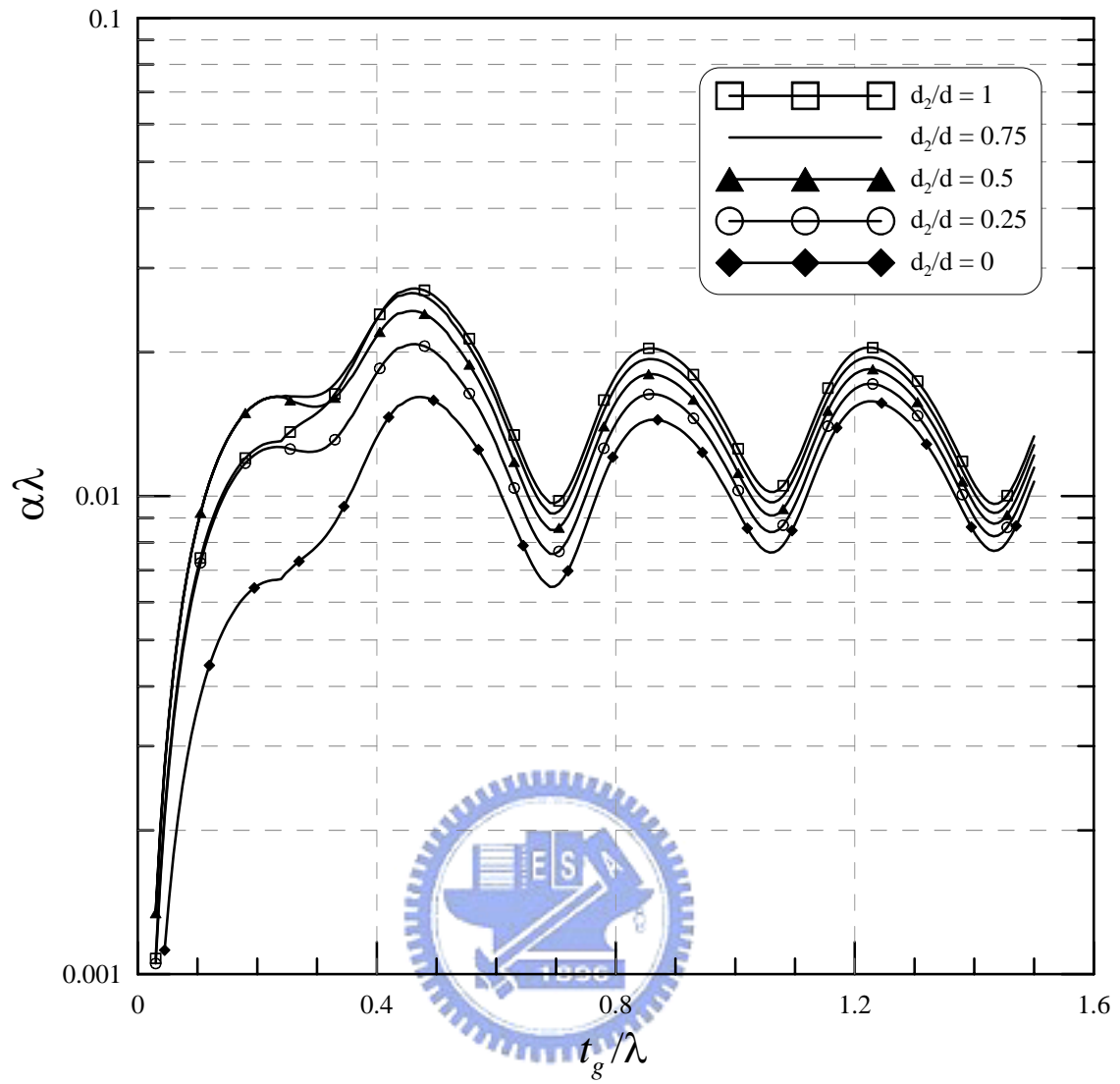


Figure 3-2(d) Variation of normalized leakage  $\alpha\lambda$  versus  $t_g/\lambda$  for the  $TE_0$  mode in symmetric gratings with the corrugated ratio of  $d_1/d = 0.25$ .

Previous literature has shown that, in the case of canonic rectangular ( $d_1/d = d_2/d = 0.5$ ) type of gratings, the leakage parameter  $\alpha$  of a grating increases monotonously with small value of  $t_g$  and is approximately proportional to  $t_g^2$ . In such a case the grating is viewed as operating in a parabolic region. On the other hand, for larger value of  $t_g$ ,  $\alpha$  oscillates periodically about a certain average value within its upper bounds and lower bounds in this saturation region. The phenomena reveal that gratings tend to exhibit a wider broadband behavior if their operation points is located at the transition between the above two regimes as shown in Figure 3-3. The design criteria for broadband couplers are determined by the operation point which depends on the grating height  $t_g$ .

Analogously to canonic rectangular gratings, the trapezoidal (triangular) ones exhibit a monotonic increase of  $\alpha\lambda$  when  $t_g$  is not too large. As  $t_g$  is increasing, the curve maintains the fluctuation except holding on a saturation level. To take it over,  $\alpha\lambda$  is decreasing. Comparing with the constant property respected to  $z$  of the perturbed dielectric constant in the rectangular case, the term  $\epsilon_{gn}$  varies as a function of  $z$  in the trapezoidal one, i.e.  $\epsilon_{gn} = \epsilon_{gn}(z)$ . For a superior choice of operation points in trapezoidal case, the transition region is also suitable for broadband operation since the curve performs a rounded change of slopes inside this interval.

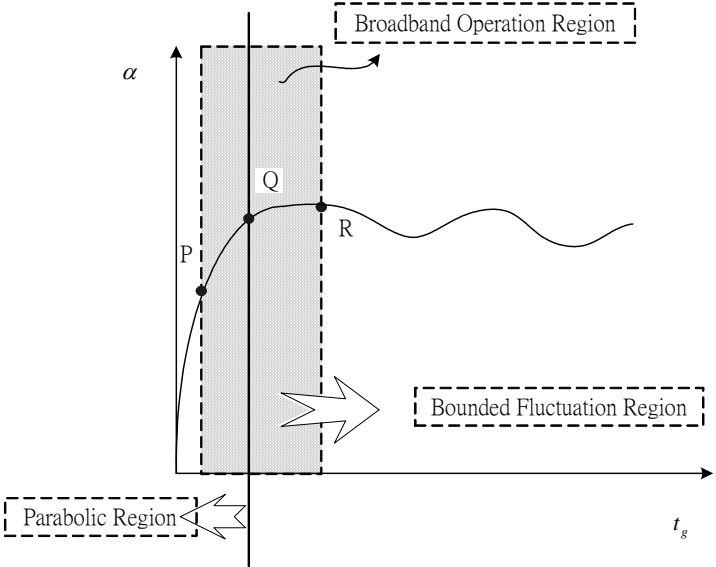


Figure 3- 3 Typical variation of the leakage  $\alpha$  versus the height  $t_g$  in a rectangular dielectric grating.

According to the work by Zhang and Tamir [16], the quadratic behavior holds well up to some points denoted by Q. The range below Q point is thus defined as parabolic region. As  $t_g$  is increasing behind the Q point, the phenomena of fluctuation rises owing to two sorts of physical mechanism. The variation of  $V_{gu}$  is still adapted due to its in-phase property with the distributed currents  $j_{-1}(z)$ . In Equation (2.29), two terms dominating this variation of  $V_{gu}$  are  $\exp(ik_{gz,-1}t_g)$  and  $\exp(2ik_{gz,-1}t_g)$ . Herein the effective wavelength in the grating layer is defined as

$$\Lambda_{g,-1} \equiv \frac{2\pi}{k_{gz,-1}} = \frac{2\pi}{\sqrt{k_0 \varepsilon_{gu} - \beta_{-1}^2}} = \frac{\lambda}{\sqrt{\varepsilon_{gu} - \left(N - \frac{\lambda}{d}\right)^2}} \quad (3.1)$$

and thus the effects of  $\exp(ik_{gz,-1}t_g)$  and  $\exp(2ik_{gz,-1}t_g)$  should be  $\Lambda_{g,-1}$  and  $\Lambda_{g,-1}/2$  respectively shown in Figure 3-2. In the structure condition we assumed, however, it can be found the results then give the period of oscillation as  $\Lambda_{g,-1}/2$ .

### 3.2 Characteristics of the Beamwidth at Broadband Operation

Due to the crossover condition of constructive and destructive phase interference generated by the above two oscillatory effects, the point Q is chosen to be one fourth of the effective wavelengths,  $\Lambda_{g,-1}/4$ , as the broadband operation point. Notice that in the mentioned figures, these points are also posited in the transition regime between parabolic and bounded saturation region and it is an appropriate regime for broadband operation because of its tender performance of the  $\alpha$  curves. In this section, we choose not only the Q points of  $\Lambda_{g,-1}/4$  but also the points P at the location of  $t_g = \Lambda_{g,-1}/8$  in the parabolic region and the points R at the location of  $t_g = \Lambda_{g,-1}/2$  respectively as noted in Figure 3-3. The considerations argue in favor of designing  $t_g$  so that these operation points act in the desired wavelength interval centered at  $\lambda_0$ . Table 3-1 shows the position of operation points while the central wavelength



Region	Parabolic	Transition	Transition interval closed to the bounded fluctuation region
$t_g$	$\frac{1}{8}\Lambda_{g,-1}$	$\frac{1}{4}\Lambda_{g,-1}$	$\frac{1}{2}\Lambda_{g,-1}$
Point	P	Q	R
for $\lambda_0 = 1550$ nm $t_g$ ( $\mu$ m)	0.1434	0.2868	0.5735

Table 3- 1 Position of broadband operation point. The center wavelength  $\lambda_0$  herein is chosen as 1550 nm.

is 1550 nm.

Generally speaking, when optical waves or electromagnetic waves are transmitting, the decay relates with the wavelength of propagating. The operation wavelength  $\lambda_0$  herein is chosen as around 1550 nm by the frequently-used one in the optical fiber communication system since it can be stimulated by the double hetero structure (DHS) such as  $\text{Ga}_x\text{In}_{1-x}\text{As}_y\text{P}_{1-y}\text{InP}$ .

In comparison with the relation between  $\alpha$  and  $t_g$  discussed in the last section, the correlation of the beamwidth  $W_{a,-1}$  of  $n = -1$  order of harmonic and  $\lambda$  exhibits the more complicated manner owing to  $N = N(\lambda)$  and  $\alpha = \alpha(\lambda)$ . However, the fluctuant mechanisms of wave interference with periodicity mentioned previously would provide to maintain  $W_{a,-1}$  as stable variation on a large interval of wavelength when a designer plans the conditions. As we discuss in Section 2.2, the beamwidth  $W_{a,-1}$  coupled into the air region is given by

$$W_{a,-1} = \frac{\cos \theta_{a,-1}}{\alpha(\lambda)} = \frac{1}{\alpha(\lambda)} \sqrt{1 - \frac{\left[ N(\lambda) - \frac{\lambda}{d} \right]^2}{\epsilon_a}} \quad (3.2A)$$

Note that Equation (3.2A) is hold while

$$1 - \frac{\left[ N(\lambda) - \frac{\lambda}{d} \right]^2}{\varepsilon_a} > 0 \quad (3.2B)$$

From Equation (3.2A), it is obvious that the beamwidth strongly depends on  $\alpha$  and the leakage factor is also a function of  $\lambda$ . As  $\lambda$  varies, the relative length  $t_g/\lambda$  is changing accordingly as well. Whenever  $t_g/\lambda$  is slight,  $\alpha\lambda$  varies correspondingly to parabolic region of  $\alpha$  versus  $t_g$  curve. As we observe in Figure 3-2,  $\alpha\lambda$  in this region has strong change as the variation of  $t_g/\lambda$ . Large values of  $t_g/\lambda$ , correspond to points in the bounded fluctuation region of  $\alpha$  versus  $t_g$  curves, belong to large-scale variation as well as points in the parabolic region. Therefore, the transition interval between those two regions should provide more stable values of  $\alpha$ .

The result for symmetric grating couplers is depicted from Figure 3-4 to 3-7. Note that all of the parameters are the same except the grating profiles. We find that the property of the beamwidth remains reasonably flat over the interval  $\Delta\lambda$  from  $1 \mu\text{m}$  to  $2 \mu\text{m}$ . While the coupler is operated at larger wavelength, the beamwidth performs slight decay since the term in Equation (3.2B) is closed to zero as  $t_g$  increases.

Regarding a broadband coupler operating at  $1550 \text{ nm}$ , Q ( $t_g = \Lambda_{g,-1}/4$ ) point provides a simple and effective design criterion. In the broadband operation region between P and R, the flatness of those curves is slightly decreasing quantitatively. Therefore, Q is not the only critical point for wideband operation. The beamwidth generated at Q point may not be a desired dimension. We finally adjust  $t_g$  to vary  $\alpha$  for satisfying the specified beamwidth as long as the operation point is not too far from Q point.

The  $n = -2$  harmonic is suppressed below  $\lambda = 1.25 \mu\text{m}$ , where the other harmonics are predicted to occur and is shown in Figure 2-2. The numerical results show that the power of the second harmonics is extremely smaller than the first harmonic and thus can be ignored.

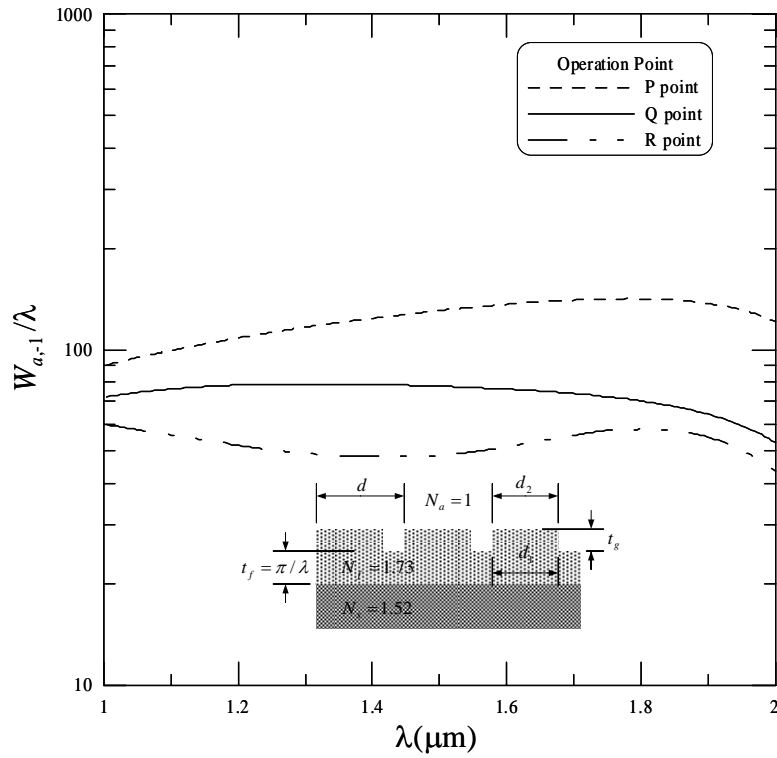


Figure 3- 4(a) Variation of  $W_{a,-1}/\lambda$  versus  $\lambda$  at points P, Q, and R for rectangular grating with aspect ratio  $d_1/d = 0.75$  and  $d_2/d = 0.75$ .

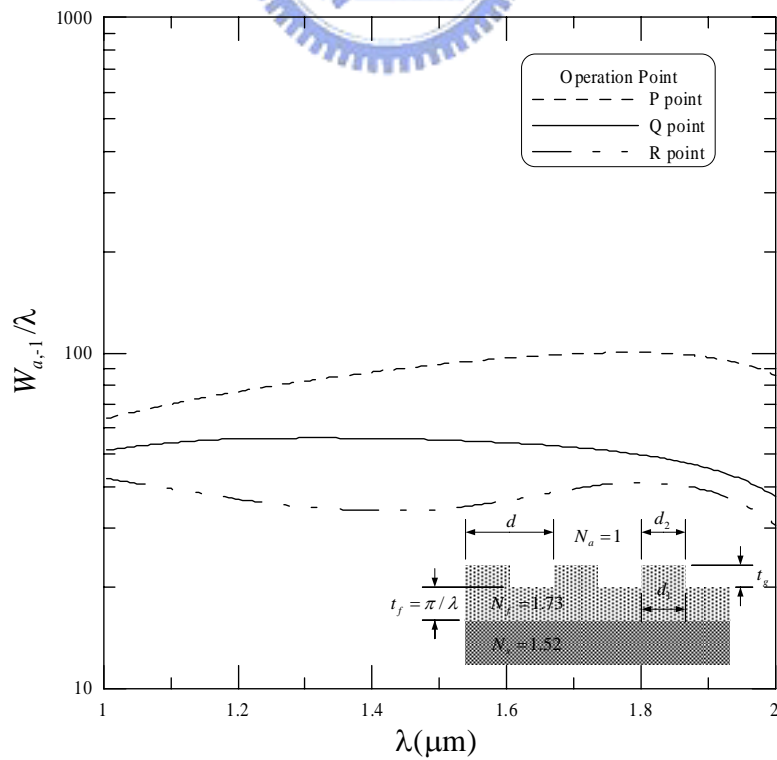


Figure 3- 4(b) Variation of  $W_{a,-1}/\lambda$  versus  $\lambda$  at points P, Q, and R for rectangular grating with aspect ratio  $d_1/d = 0.5$  and  $d_2/d = 0.5$ .

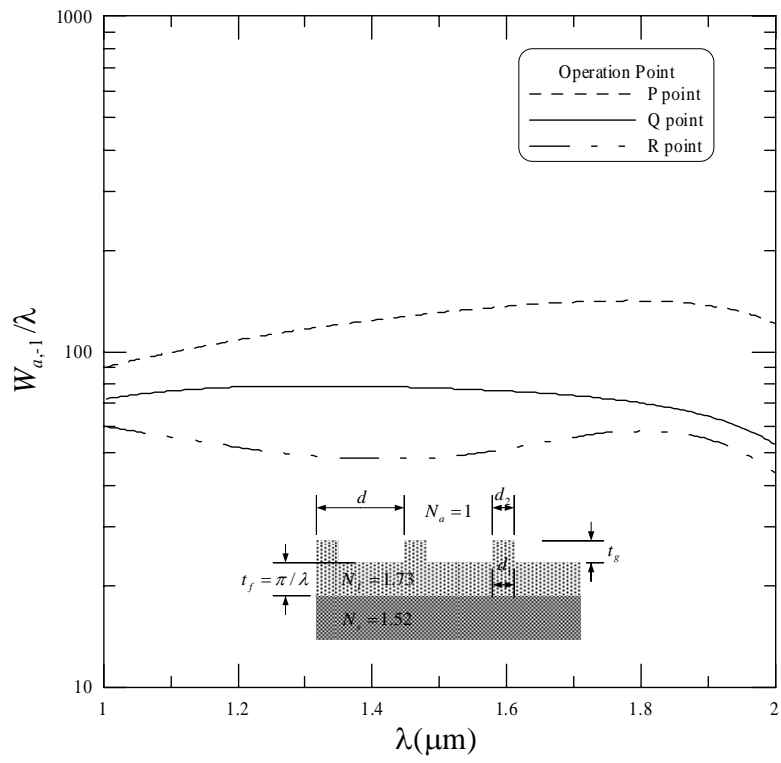
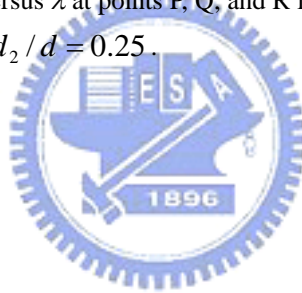


Figure 3- 4(c) Variation of  $W_{a,-1}/\lambda$  versus  $\lambda$  at points P, Q, and R for rectangular grating with aspect ratio  $d_1/d = 0.25$  and  $d_2/d = 0.25$ .



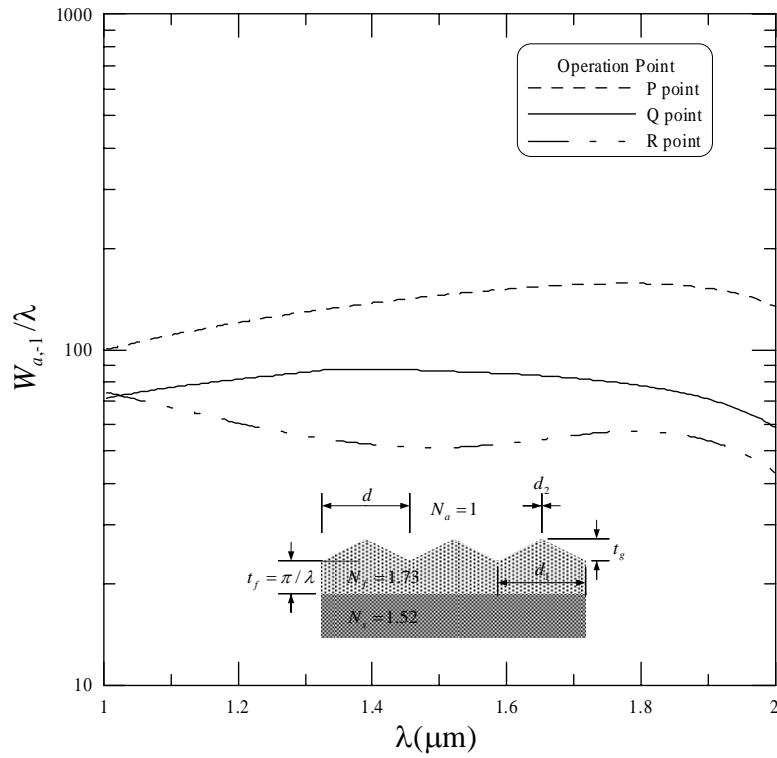


Figure 3- 5 (a) Variation of  $W_{a,-1}/\lambda$  versus  $\lambda$  at points P, Q, and R for symmetric triangular grating with aspect ratio  $d_1/d = 1$  and  $d_2/d = 0$ .

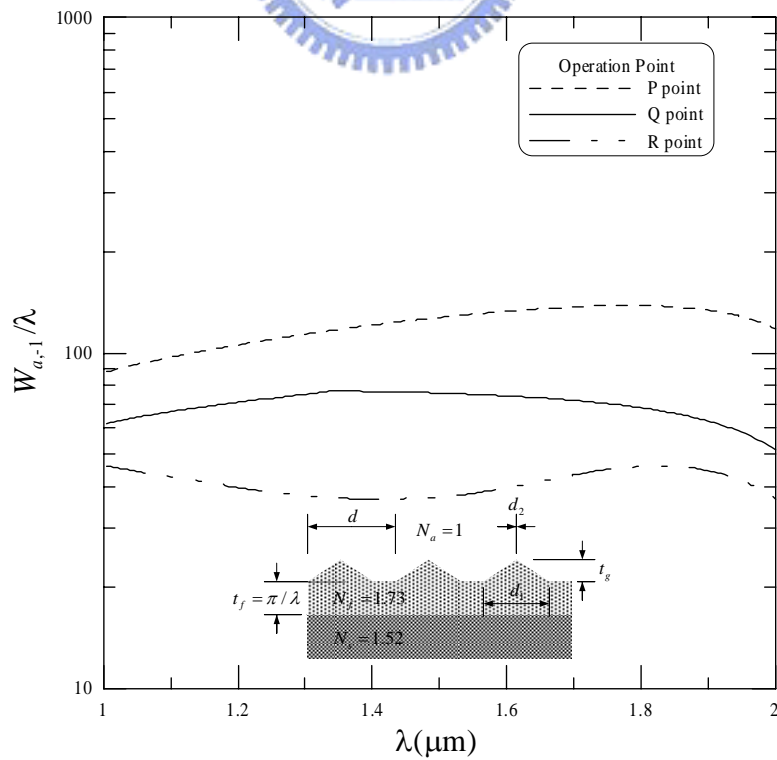


Figure 3- 5(b) Variation of  $W_{a,-1}/\lambda$  versus  $\lambda$  at points P, Q, and R for symmetric triangular grating with aspect ratio  $d_1/d = 0.75$  and  $d_2/d = 0$ .

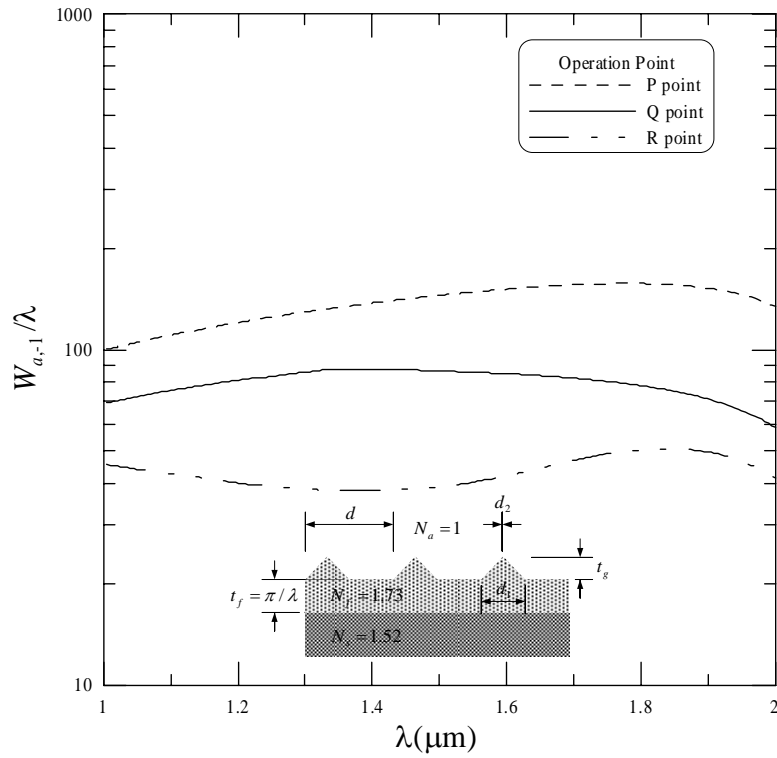


Figure 3- 5(c) Variation of  $W_{a,-1}/\lambda$  versus  $\lambda$  at points P, Q, and R for symmetric triangular grating with aspect ratio  $d_1/d = 0.5$  and  $d_2/d = 0$ .

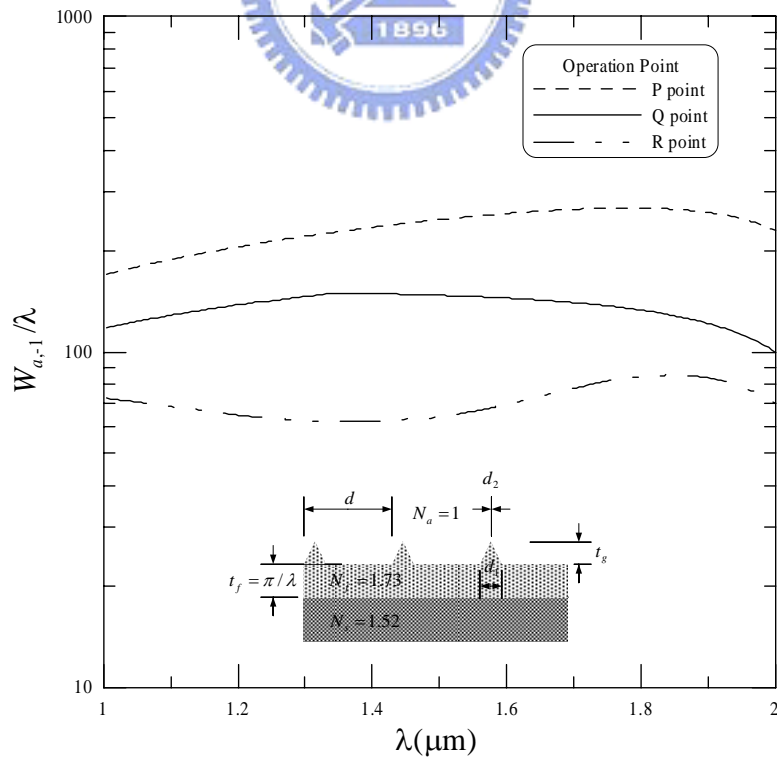


Figure 3- 5(d) Variation of  $W_{a,-1}/\lambda$  versus  $\lambda$  at points P, Q, and R for symmetric triangular grating with aspect ratio  $d_1/d = 0.25$  and  $d_2/d = 0$ .

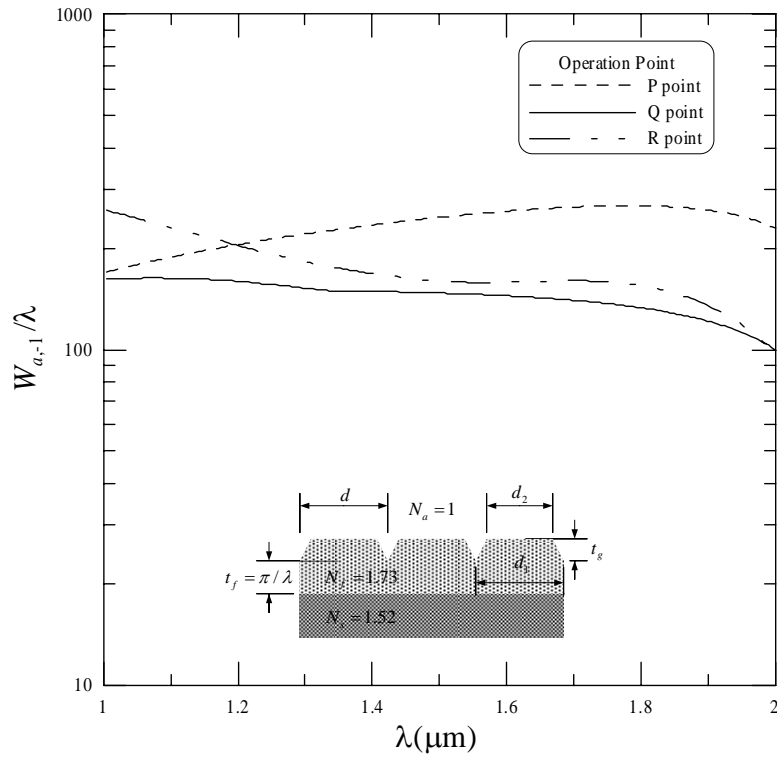


Figure 3- 6(a.1) Variation of  $W_{a,-1}/\lambda$  versus  $\lambda$  at points P, Q, and R for the regular trapezoidal gratings with aspect ratio  $d_1/d = 1$  and  $d_2/d = 0.75$ .

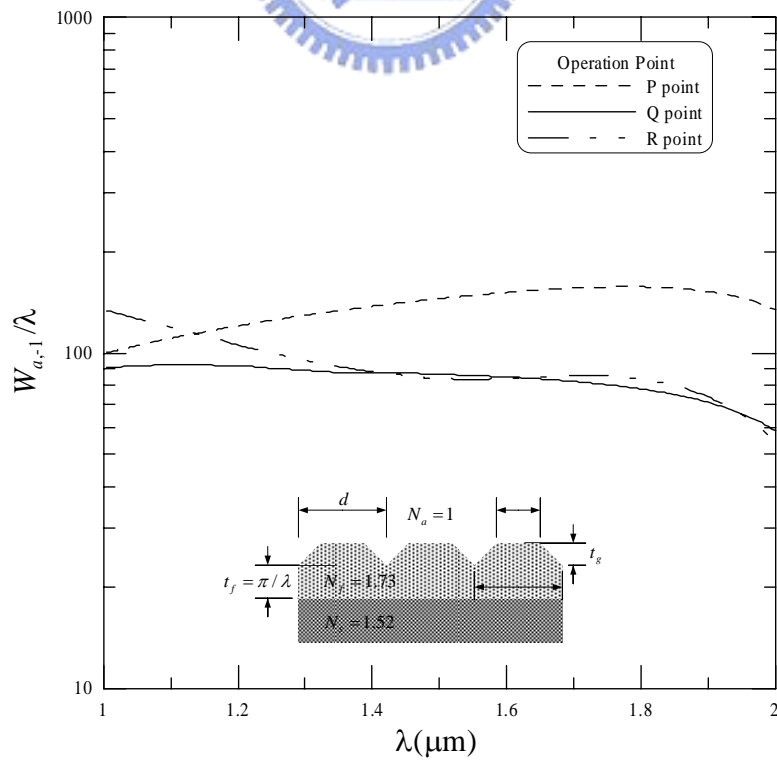


Figure 3- 6(a.2) Variation of  $W_{a,-1}/\lambda$  versus  $\lambda$  at points P, Q, and R for the regular trapezoidal gratings with aspect ratio  $d_1/d = 1$  and  $d_2/d = 0.5$ .

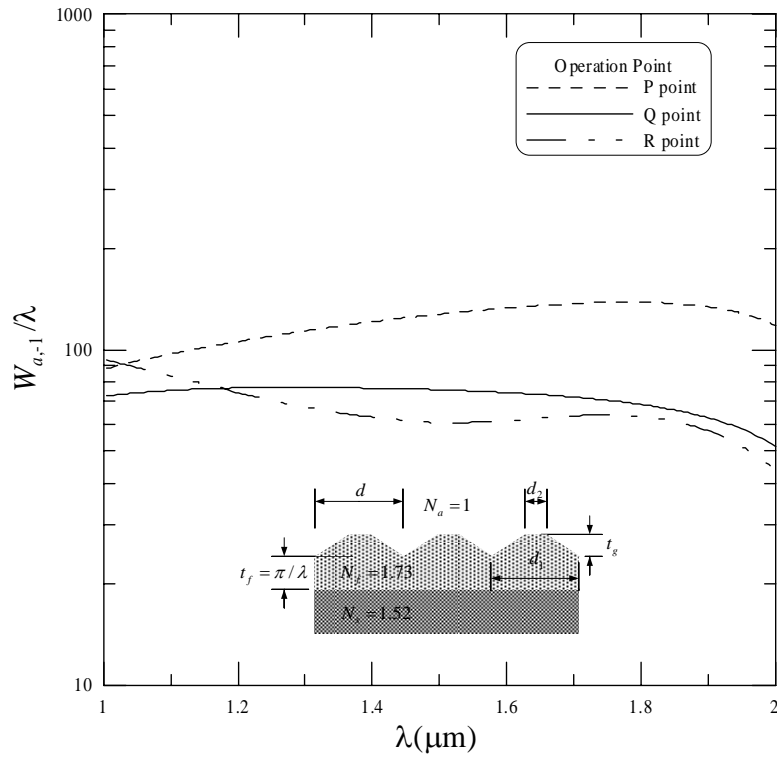


Figure 3- 6(a.3) Variation of  $W_{a,-1}/\lambda$  versus  $\lambda$  at points P, Q, and R for the regular trapezoidal gratings with aspect ratio  $d_1/d = 1$  and  $d_2/d = 0.25$ .

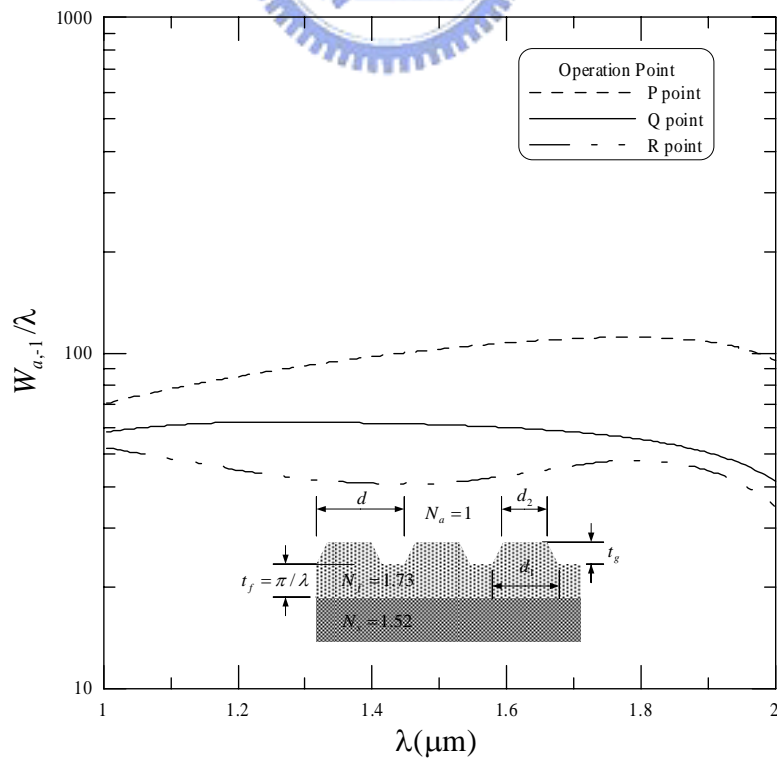


Figure 3- 6(b.1) Variation of  $W_{a,-1}/\lambda$  versus  $\lambda$  at points P, Q, and R for the regular trapezoidal gratings with aspect ratio  $d_1/d = 0.75$  and  $d_2/d = 0.5$ .



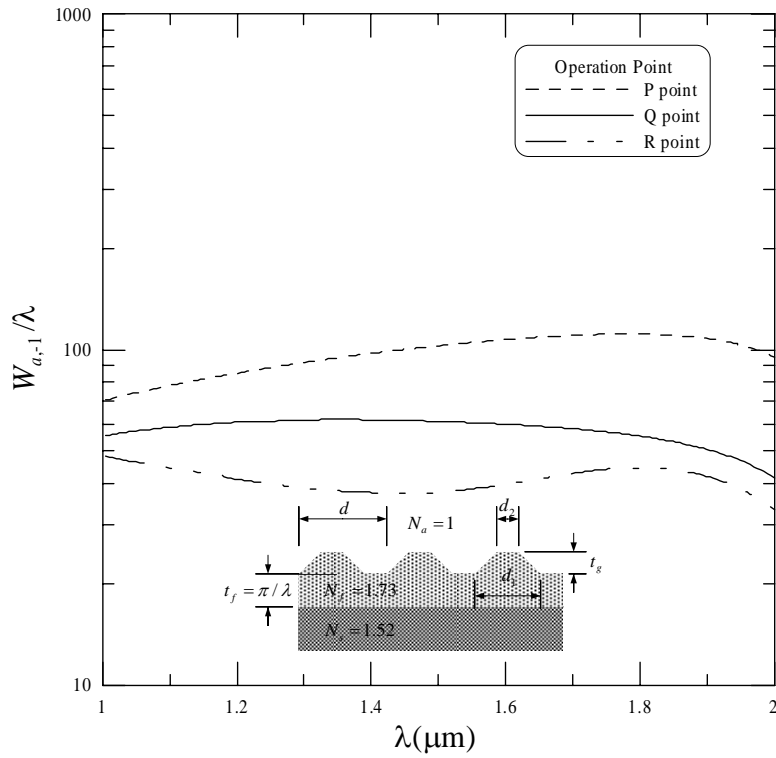


Figure 3- 6(b.2) Variation of  $W_{a,-1}/\lambda$  versus  $\lambda$  at points P, Q, and R for the regular trapezoidal gratings with aspect ratio  $d_1/d = 0.75$  and  $d_2/d = 0.25$ .

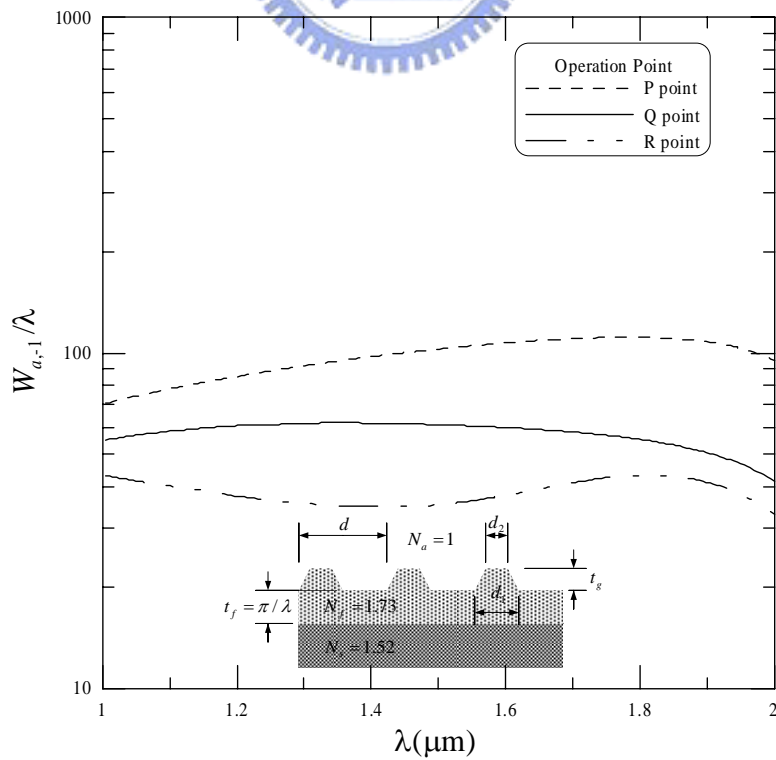


Figure 3- 6(c) Variation of  $W_{a,-1}/\lambda$  versus  $\lambda$  at points P, Q, and R for the regular trapezoidal gratings with aspect ratio  $d_1/d = 0.5$  and  $d_2/d = 0.25$ .

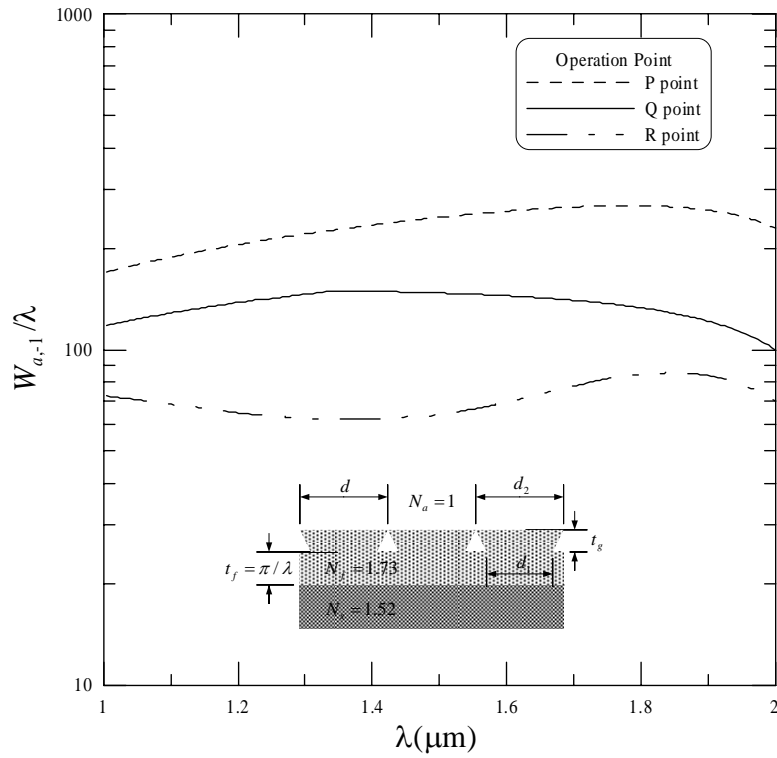


Figure 3- 7(a) Variation of  $W_{a,-1}/\lambda$  versus  $\lambda$  at points P, Q, and R for the inverse trapezoidal gratings with aspect ratio  $d_1/d = 0.75$  and  $d_2/d = 1$ .

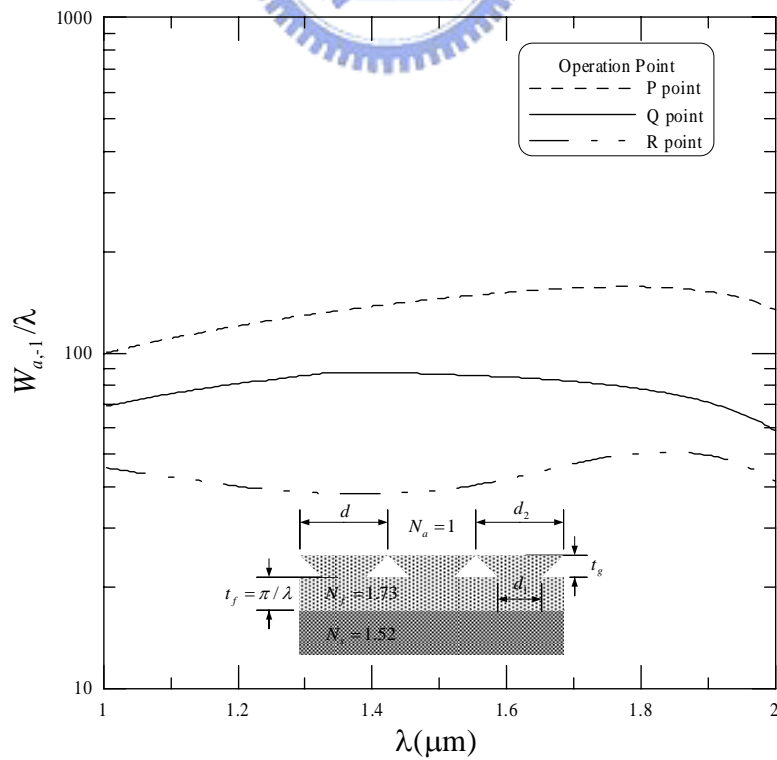


Figure 3- 7(b.1) Variation of  $W_{a,-1}/\lambda$  versus  $\lambda$  at points P, Q, and R for the inverse trapezoidal gratings with aspect ratio  $d_1/d = 0.5$  and  $d_2/d = 1$ .

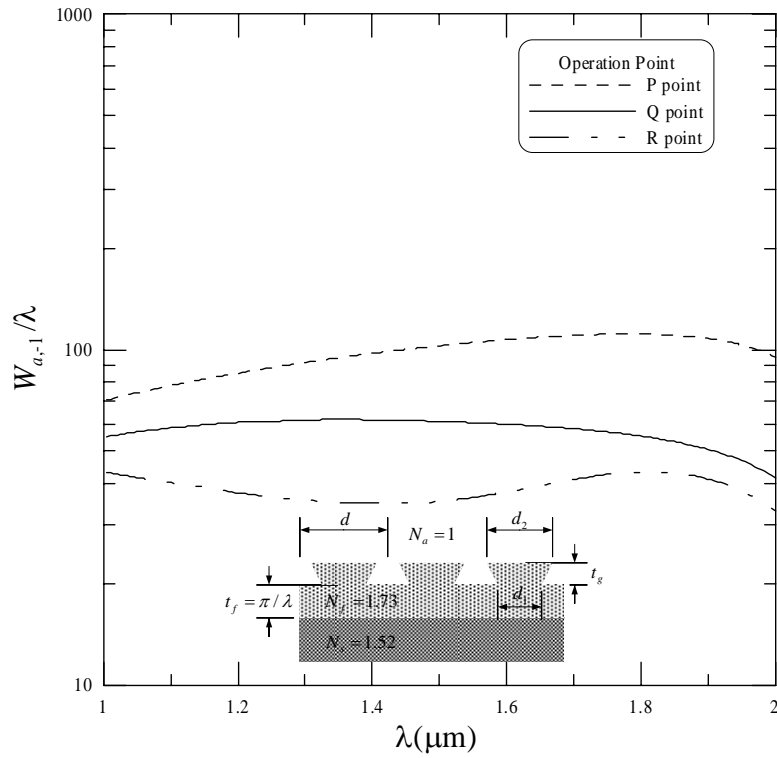


Figure 3- 7(b.2) Variation of  $W_{a,-1}/\lambda$  versus  $\lambda$  at points P, Q, and R for the inverse trapezoidal gratings with aspect ratio  $d_1/d = 0.5$  and  $d_2/d = 0.75$ .

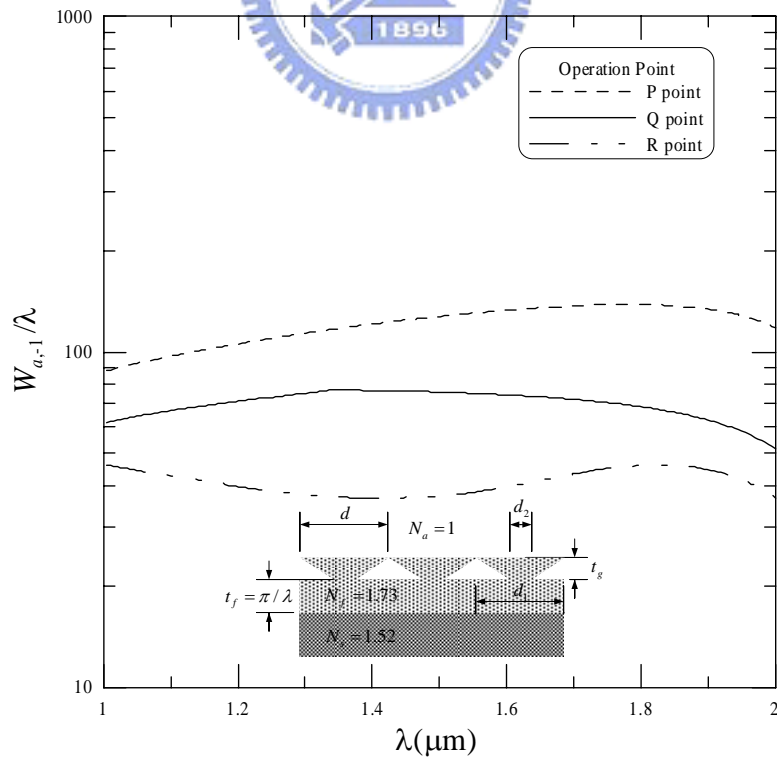


Figure 3- 7(c.1) Variation of  $W_{a,-1}/\lambda$  versus  $\lambda$  at points P, Q, and R for the inverse trapezoidal gratings with aspect ratio  $d_1/d = 0.25$  and  $d_2/d = 1$ .

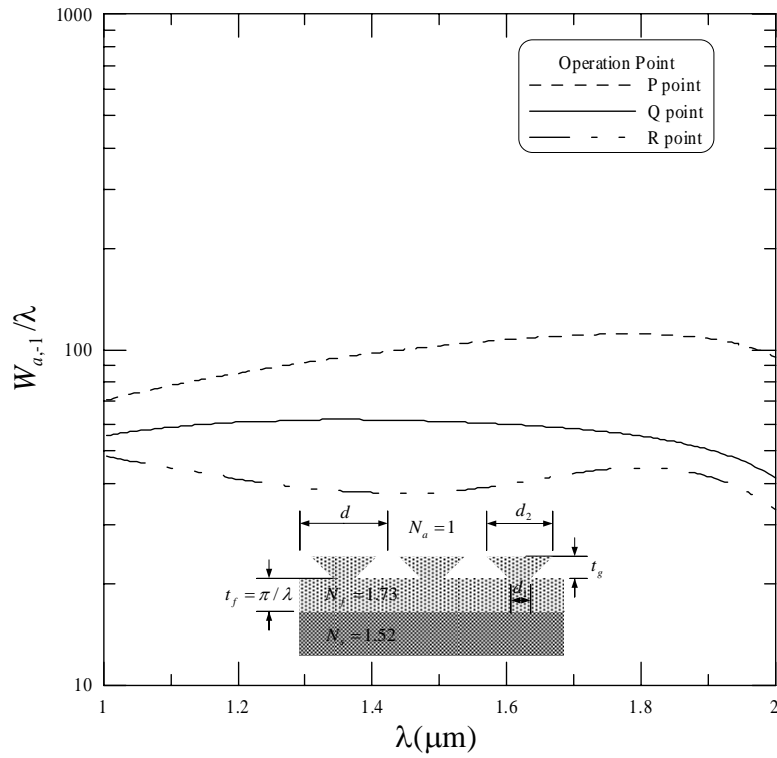


Figure 3- 7(c.2) Variation of  $W_{a,-1}/\lambda$  versus  $\lambda$  at points P, Q, and R for the inverse trapezoidal gratings with aspect ratio  $d_1/d = 0.25$  and  $d_2/d = 0.75$ .

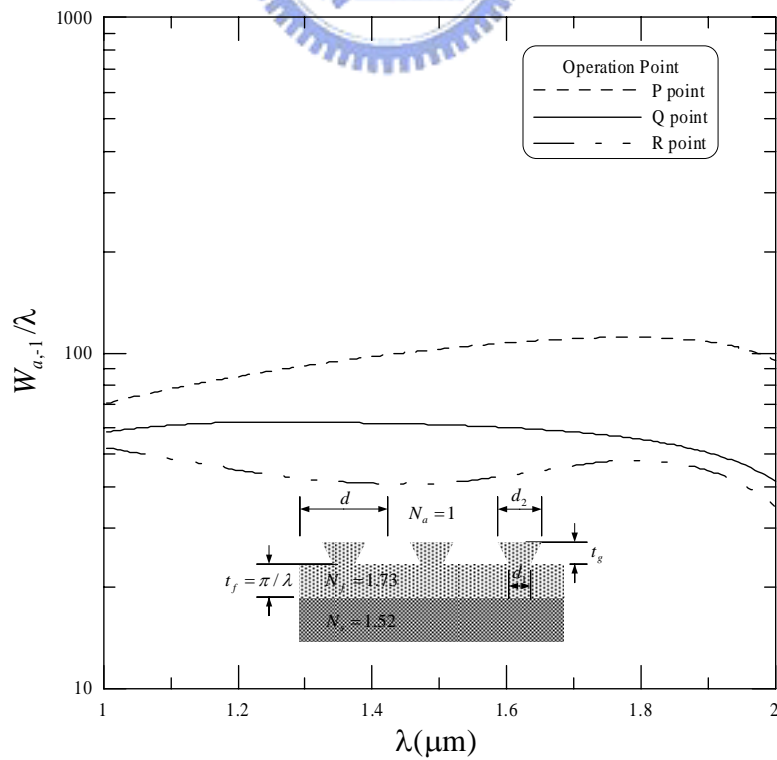
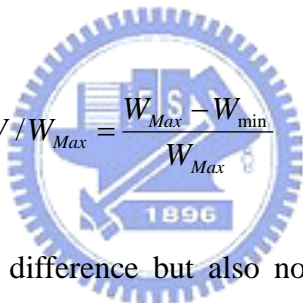


Figure 3- 7(c.3) Variation of  $W_{a,-1}/\lambda$  versus  $\lambda$  at points P, Q, and R for the inverse trapezoidal gratings with aspect ratio  $d_1/d = 0.25$  and  $d_2/d = 0.5$ .

### 3.3 Discussion on variation of beamwidth on $\Delta\lambda$ for different profile

The beamwidth property of each shape of grating is shown in the last section. To contrast the flatness of those profiles, we introduce two terms, the area  $\Delta$  and the fractional beamwidth  $\Delta W / W_{Max}$ , are shown in Figure 3-8. For the submicron technology, the fabrication tolerance of grating height  $t_g$  must be discussed with wideband operation. These two terms, however, help to determine the connection between the grating height and variation of beamwidth over a wavelength band  $\Delta\lambda$  form  $1\mu\text{m}$  to  $2\mu\text{m}$ .

The area  $\Delta$ , henceforth, indicates the scanning of the beamwidth variation as  $t_g$  is changing, and roughly the smaller  $\Delta$  is, the flatter the variation of beamwidth is. Nevertheless,  $\Delta$  only exhibits the difference of beamwidth absolutely and is independent of the operation beamwidth. The other term,  $\Delta W / W_{Max}$ , defined as

$$\Delta W / W_{Max} = \frac{W_{Max} - W_{min}}{W_{Max}} \quad (3.3)$$


is not only considered about the difference but also normalized to the largest beamwidth relatively. Thus, for the case with larger  $W_{Max}$  and unitary beamwidth difference, the term performs a smaller value and hence reveals the lower fraction of the beamwidth.

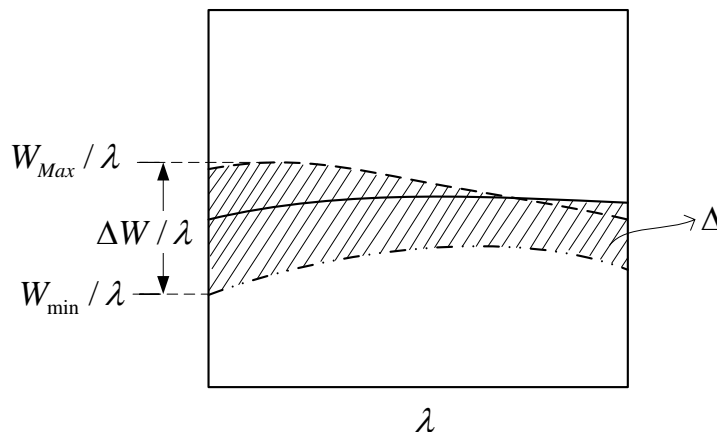


Figure 3- 8 Typical variation of the normalized beamwidth  $W / \lambda$  versus wavelength

$[d_1/d, d_2/d]$	[0.75,0.75]	[0.5,0.5]	[0.25,0.25]
$\Delta$	72.0055	50.9157	72.0055
$\Delta W/W_{Max}$	0.6996	0.6996	0.6996

Table 3- 2(a)  $\Delta$  and  $\Delta W/W_{Max}$  in rectangular gratings.

$[d_1/d, d_2/d]$	[1,0]	[0.75,0]	[0.5,0]	[0.25,0]
$\Delta$	82.0125	80.5991	95.1744	164.9242
$\Delta W/W_{Max}$	0.732	0.7385	0.7591	0.7694

Table 3- 2(b)  $\Delta$  and  $\Delta W/W_{Max}$  in symmetric triangular gratings.

$[d_1/d, d_2/d]$	[1,0.75]	[1,0.5]	[1,0.25]	[0.75,0.5]	[0.75,0.25]	[0.5,0.25]
$\Delta$	100.2802	57.2929	57.0842	53.5352	56.8849	59.3
$\Delta W/W_{Max}$	0.6437	0.6612	0.6905	0.6928	0.7067	0.7094

Table 3- 2(c)  $\Delta$  and  $\Delta W/W_{Max}$  in regular trapezoidal gratings.

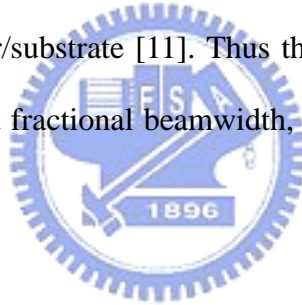
$[d_1/d, d_2/d]$	[0.75,1]	[0.5,1]	[0.5,0.75]	[0.25,1]	[0.25,0.75]	[0.25,0.5]
$\Delta$	164.9242	95.1744	59.3	80.5991	56.8849	53.5352
$\Delta W/W_{Max}$	0.7694	0.7591	0.7094	0.7385	0.7067	0.6928

Table 3- 2(d)  $\Delta$  and  $\Delta W/W_{Max}$  in inverse trapezoidal gratings.

Table 3-2 exhibits  $\Delta$  and  $\Delta W/W_{Max}$  in different types of grating shape. In the viewpoint of  $\Delta$ , we first find the canonic rectangular ( $d_1/d = d_2/d = 0.5$ ) structure has the smallest area. It verifies the canonic rectangular gratings can offer wider bandwidths and flatter beamwidth over a fixed wavelength band than any other type of grating. The regular trapezoidal types and inverse ones also provide the areas which are not too far from which the canonic rectangular gratings provide. Observe the cases of trapezoidal shape with  $d_1/d = 1$  in Figure 3.5(a), 3.6(a.1), 3.6(a.2) and 3.6(a.3), there the crosses between two curves exist and they would reduce the difference of variation and thus decrease  $\Delta$ . However, it can be found obviously that symmetric triangular profiles have larger areas than all the others. In Figure 3-2(a)-(d), the  $\alpha$  curves of triangular profile are almost sharper and smaller than other curve of profiles and it would cause their beamwidth is generally larger and decrease its broadband

flatness. Oppositely, the cases of  $[d_1/d = 0.25, d_2/d = 0]$  (symmetric triangular) and  $[d_1/d = 0.75, d_2/d = 1]$  (regular trapezoidal), which geometry are complementary to each other, would exhibit worst evenness.

Regular trapezoidal gratings commonly remain small values of the fractional beamwidth  $\Delta W/W_{Max}$  as we observe due to their larger  $W_{Max}$  in denominator. The canonic rectangular grating also performs a low value of the fractional beamwidth with acceptancy. Specifically, something interesting is that the fractional beamwidth of the three rectangular cases are equal despite of different  $\Delta W$ ,  $W_{Max}$  and  $W_{min}$ . Though the symmetric triangular gratings have larger  $W_{Max}$ , their  $\Delta W/W_{Max}$  are not small as we expect. The group of triangular shapes still behaves larger variation on flatness and may have less application on broadband operations. Fortunately, triangular gratings with asymmetry, such as blazed dielectric ones, promote the power efficiency leaked to the air/substrate [11]. Thus the gratings with canonic rectangular profiles, which have low area and fractional beamwidth, are more appropriate for broadband operation in our discussion.



# Chapter IV

## Conclusion

---

The dielectric gratings can be designed to deliver out-coupled beams with reasonably constant widths and intensities over a large wavelength interval  $\Delta\lambda$ . Specifically, types of gratings with grating height  $t_g$  around  $\Lambda_{g,-1}/4$  convert a surface-wave into a leaky beam which beamwidth is remained flat over a wavelength band from  $1\mu\text{m}$  to  $2\mu\text{m}$ . The performances of other choices of  $t_g$  such as  $\Lambda_{g,-1}/2$  or  $\Lambda_{g,-1}/8$  vary slightly but still maintain the evenness condition in the wavelength interval. The flexibility of  $t_g$  therefore provides the broadband operation region of desired beamwidth, and then a new design criterion can be concluded.

Furthermore, the analysis of the flatness for different types of gratings shows canonic rectangular grating has the smallest variation, i.e. most flatness, due to the lowest area  $\Delta$ . This property is appropriate for wideband application and provides the tolerance for the deficiency of fabrications. On the other hand, symmetric triangular ones commonly present small values not only on area  $\Delta$  but also the fractional beamwidth  $\Delta W/W_{Max}$ . In comparison with symmetric triangular gratings, rectangular or trapezoidal ones have better evenness.

Originally, the order of  $n = -2$  harmonic is excited according to the linear programming diagram of  $N = \beta_{sw}/k_0$  versus  $\lambda/d$ . Because of the symmetrical structures as we introduced, the power of the second harmonic is restricted to be very small, and therefore the power leaked out to the air/substrate is almost not influenced by that little portion so that the spectrum properties can retain a flat condition as designers' expectation.

Small perturbation method provides an acceptable accuracy and efficient calculation for computers in comparison with the rigorous method which need elaborate numerical computations while the grating height  $t_g$  is selected on the transition region between the



parabolic regime and bounded saturation regime. Thus, because of the simplicity in formulations, this method is appropriate to broadband analysis. Quantitatively, the higher order modes exhibit more violent oscillation than the fundamental one. It is expected that they have less wideband behavior than a fundamental  $TE_0$  mode does.



# Bibliography

---

- [1] T. Tamir, *Integrated Optics*, Springer-Verlag, ch. 3, pp. 110-118, 1985.
- [2] H. Nishihara, M. Haruna and T. Suhara, *Optical Integrated Circuits*, McGraw-Hill, pp. 62-94, 1989.
- [3] R. E. Collin and F. J. Zucker, *Antenna theory*, part 2, McGraw-Hill, pp.184-188, 1969.
- [4] A. Ishimaru, *Electromagnetic wave propagation, radiation, and scattering*, Prentice-Hall, pp.178-180, 1991.
- [5] R. E Collin, *Field theory of guided waves*, IEEE Press, pp. 605-608, 1991.
- [6] L. B. Felsen and N. Marcuvitz, *Radiation and scattering of waves*, Prentice-Hall, pp.185, 1973.
- [7] T. Tamir and S. T. Peng, "Analysis and design of grating couplers," *Appl. Phys.*, vol. 14, pp. 69-73, 1977.
- [8] F. T. Stone and S. Austin, "A theoretical and experimental study of the effect of loss on grating couplers," *IEEE J. Quantum Electron.*, vol. QE-12, No. 11, pp. 727-732, Nov. 1976.
- [9] K. Handa, S.T. Peng and T. Tamir, "Improved perturbation analysis of dielectric gratings," *Appl. Phys.*, vol.5, pp.325-328, 1975.
- [10] M. D. Salik, P. Chavel, "Resonant excitation analysis of waveguide grating couplers," *Opt. Commun.*, vol.193, pp.127-131, 2001.
- [11] K. C. Chang and T. Tamir, "Simplified approach to surface-wave scattering by blazed dielectric gratings," *Appl. Phys.*, vol.19, no.2, pp.282-288, 1980.
- [12] S. T. Peng, "Rigorous formulation of scattering and guidance by dielectric grating waveguide: general case of oblique incidence," *J. Opt. Soc. Am.*, vol.6, pp.1869-1883, 1989.
- [13] R. B. Hwang and Ching-Chuan Wei, "Small perturbation analysis of diffracted holographic gratings," *Opt. Commun.*, 125, pp.217-221, 1996.
- [14] R. B. Hwang and D. K. Jen, "Small perturbation analysis of diffracted holographic gratings," *Microwave and optical technology letters*, vol.19, no.6, pp.434-437, Dec. 1998.
- [15] K. C. Chang, V. Shah, and T. Tamir, "Scattering and guiding of waves by dielectric gratings with arbitrary profiles," *J. Opt. Soc. Am.*, vol.70, pp.804-813, 1980.
- [16] S. Zhang and T. Tamir, "Analysis and design of broadband grating couplers," *IEEE J. Quantum Electron.*, vol. 29, No. 11, pp. 2813-2824, Nov. 1993.
- [17] R. M. Emmons and D. G. Hall, "Buried-oxide silicon-on insulator structures-II: Waveguide grating couplers," *J. Quantum Electron.*, vol. 28, pp. 164-175, Nov. 1992.
- [18] R. M. Emmons and D. G. Hall, "Comparison of film thickness tolerances in waveguide grating couplers," *Opt. Lett.*, vol. 16, pp.998-1000, 1992.
- [19] K. Ogawa and W. S. C. Chang, "Analysis of Holographic thin film grating coupler," *Appl. Optics.*, vol.12, no. 9, pp.2167-2171, 1973.
- [20] S. T. Peng, H. L. Bertoni and T. Tamir, "Analysis of periodic thin film structures with rectangular profiles," *Optics Commun.*, vol. 10, no.1, Jan 1974.

- [21] S. T. Peng, T. Tamir and H. L. Bertoni, "Theory of periodic dielectric waveguides," *IEEE Trans. M.T.T.*, vol. MTT-23, pp. 123-133, Nov. 1975.

